CDK10 Mutations in Humans and Mice Cause Severe Growth Retardation, Spine Malformations, and Developmental Delays

Christian Windpassinger,[1,25] Juliette Piard,[2,22,25] Carine Bonnard,[3,25] Majid Alfadhel,[4,25] Shuhui Lim,[5,23,25] Xavier Bisteau,[5] Stéphane Blouin,[6] Nur'Ain B. Ali,[3] Alvin Yu Jin Ng,[5] Hao Lu,[5] Sumanty Tohari,[5] S. Zakiah A. Talib,[5] Noémi van Hul,[5] Matias J. Caldez,[5,7] Lionel Van Maldergem,[2,22] Gökhan Yigit,[8] Hülya Kayserili,[9] Sameh A. Youssef,[10] Vincenzo Coppola,[11,24] Alain de Bruin,[10] Lino Tessarollo,[11] Hyungwon Choi,[5,12] Verena Rupp,[1] Katharina Roetzer,[6,13,14] Paul Roschger,[6] Klaus Klaushofer,[6] Janine Altmüller,[15] Sudipto Roy,[5,16,17] Byrappa Venkatesh,[5,16] Rudolf Ganger,[18] Franz Grill,[18] Farid Ben Chehida,[19] Bernd Wollnik,[8] Umut Altunoglu,[20] Ali Al Kaissi,[6,18,26] Bruno Reversade,[3,5,9,16,21,26,*] and Philipp Kaldis[5,7,26,*]

In five separate families, we identified nine individuals affected by a previously unidentified syndrome characterized by growth retardation, spine malformation, facial dysmorphisms, and developmental delays. Using homozygosity mapping, array CGH, and exome sequencing, we uncovered bi-allelic loss-of-function *CDK10* mutations segregating with this disease. CDK10 is a protein kinase that partners with cyclin M to phosphorylate substrates such as ETS2 and PKN2 in order to modulate cellular growth. To validate and model the pathogenicity of these *CDK10* germline mutations, we generated conditional-knockout mice. Homozygous *Cdk10*-knockout mice died postnatally with severe growth retardation, skeletal defects, and kidney and lung abnormalities, symptoms that partly resemble the disease's effect in humans. Fibroblasts derived from affected individuals and *Cdk10*-knockout mouse embryonic fibroblasts (MEFs) proliferated normally; however, *Cdk10*-knockout MEFs developed longer cilia. Comparative transcriptomic analysis of mutant and wild-type mouse organs revealed lipid metabolic changes consistent with growth impairment and altered ciliogenesis in the absence of CDK10. Our results document the CDK10 loss-of-function phenotype and point to a function for CDK10 in transducing signals received at the primary cilia to sustain embryonic and postnatal development.

Introduction

Individuals with severe growth retardation arising from developmental defects often suffer from additional medical problems that make diagnosing these diseases difficult. Here, we studied nine individuals (from five families) who display a closely matched array of phenotypes characterized by severe growth retardation, spine malformation, facial dysmorphisms, developmental delay, and intellectual disability. Using next-generation sequencing, we discovered that all affected individuals harbor germline homozygous mutations in cyclin-dependent kinase 10 (*CDK10* [MIM: 603464]).

Consisting of 20 members in mammals, the group of protein kinases known as CDKs play critical roles in cell-cycle control, transcription, and development.[1,2] CDKs (CDK1–CDK6) mostly promote the progression from one cell-cycle phase to the next, and CDK1 is essential for

[1]Institute of Human Genetics, Medical University of Graz, 8010 Graz, Austria; [2]Centre de Génétique Humaine, Centre Hospitalier Universitaire Besançon, 25030 Besançon, France; [3]Institute of Medical Biology, Agency for Science, Technology, and Research, Singapore 138648, Republic of Singapore; [4]King Abdullah International Medical Research Centre, King Saud bin Abdulaziz University for Health Sciences, Division of Genetics, Department of Pediatrics, King Abdulaziz Medical City, Ministry of National Guard-Health Affairs, Riyadh 11481, Saudi Arabia; [5]Institute of Molecular and Cell Biology, Agency for Science, Technology, and Research, 61 Biopolis Drive, Singapore 138673, Republic of Singapore; [6]Ludwig Boltzmann Institute of Osteology at the Hanusch Hospital of WGKK and AUVA Trauma Centre Meidling, 1st Medical Department, Hanusch Hospital, Heinrich-Collin-Strasse 30, 1140 Vienna, Austria; [7]National University of Singapore, Department of Biochemistry, Singapore 117597, Republic of Singapore; [8]Institute of Human Genetics, University Medical Center Göttingen, 37099 Göttingen, Germany; [9]Department of Medical Genetics, Koç University, School of Medicine, 34010 Topkapı, Istanbul, Turkey; [10]Department of Pathobiology, Faculty of Veterinary Medicine, Utrecht University, 3584 CL Utrecht, the Netherlands; [11]National Cancer Institute, Mouse Cancer Genetics Program, NCI Frederick, Building 560, 1050 Boyles Street, Frederick, MD 21702-1201, USA; [12]Saw Swee Hock School of Public Health, National University Singapore, Singapore National University Health System, Singapore 117549, Republic of Singapore; [13]Center for Medical Genetics, Hanusch Hospital, Heinrich-Collin-Strasse 30, 1140 Vienna, Austria; [14]Sigmund Freud Private University, Medical School, Freudplatz 1, 1020 Vienna, Austria; [15]Cologne Center for Genomics, University of Cologne, Weyertal 115b, 50931 Cologne, Germany; [16]Department of Paediatrics, School of Medicine, National University of Singapore, Singapore 119228, Republic of Singapore; [17]Department of Biological Sciences, National University of Singapore, Singapore 117558, Republic of Singapore; [18]Orthopedic Hospital of Speising, Speisinger Strasse 109, 1130 Vienna, Austria; [19]Center of Radiology, Department of Imaging Studies-Ibn Zohr Institute, Tunis, City Khadra 1003, Tunisia; [20]Medical Genetics Department, Istanbul Medical Faculty, Istanbul University, 34093 Istanbul, Turkey; [21]Amsterdam Reproduction & Development, Academic Medical Centre & VU University Medical Center, Meibergdreef 9, 1105 AZ Amsterdam, the Netherlands; [22]Integrative and Cognitive Neuroscience Research Unit EA481, Université de Franche-Comté, 25030 Besançon, France
[23]Present address: Translational Medicine Research Center, Merck Research Laboratories, Singapore 138665, Republic of Singapore
[24]Present address: The Ohio State University, Department of Molecular Virology, Immunology, and Medical Genetics, 988 Biomedical Research Tower, 460 West 12th Ave., Columbus, OH 43210, USA
[25]These authors contributed equally to this work
[26]These authors contributed equally to this work
*Correspondence: bruno@reversade.com (B.R.), kaldis@imcb.a-star.edu.sg (P.K.)
http://dx.doi.org/10.1016/j.ajhg.2017.08.003.

proliferation. CDKs have been characterized extensively, and some of their substrates and in vivo functions are known.[1,3] Another group of CDKs, e.g., CDK7–CDK9 and CDK11–CDK13, are mostly involved in transcription. Most of the remaining CDKs are "orphan" kinases, which have been poorly studied. CDK10 is an orphan kinase that was cloned on the basis of its homology to CDK1.[4,5] CDK10 binds the transcription factor ETS2 and modulates its transactivation.[6] CDK10 kinase activity is regulated by the binding of CDK10 to cyclin M, which is the product of *FAM58A* (MIM: 300708).[7] CDK10/cyclin M complexes also have been shown to phosphorylate ETS2, leading directly to degradation of ETS2. X-linked mutations in *FAM58A* have been reported to cause STAR syndrome (MIM: 300707).[8,9] Recently, it was revealed that CDK10/cyclin M complexes phosphorylate the protein kinase PKN2, which affects cilia growth.[10] In zebrafish, morpholino-mediated silencing of *cdk10* impaired neurogenesis by modulating *raf1a* expression.[11] In addition, *CDK10* was one locus implicated by a genome-wide association study (GWAS) for determining height in Han Chinese.[12]

Germline mutations in CDK genes are exceedingly rare with the exception of an activating germline mutation (encoding p.Arg24Cys) predisposing to malignant melanoma[13,14] in *CDK4* (MIM: 123829) and *CDK6* mutations that cause autosomal-recessive primary microcephaly 12 (MCPH12 [MIM: 616080]).[15] To the best of our knowledge, no other loss-of-function mutations in any member of the CDK family have been linked to a Mendelian syndrome.

Material and Methods

Array CGH Analysis

The Human Genome CGH Microarray Kit 180k (Agilent Technologies) was used according to the manufacturer's instructions. The data were analyzed by Agilent Cytogenomics software with the statistical algorithm ADM-2 and a 3-probe minimum aberration call and were compared with the Database of Genomic Variants. Coordinates of copy-number variations are based on the GRCh36/hg18 assembly.

Exome Sequencing

The exome library was prepared on an Ion OneTouch System and sequenced on an Ion Proton instrument (Life Technologies) with one Ion PI chip. Sequence reads were aligned to the human GRCh37/hg19 assembly (UCSC Genome Browser). Variants were filtered for common SNPs against the NCBI's "common and no known medical impacts" database (ClinVar), the Exome Aggregation Consortium (ExAC) Browser, the NHLBI Exome Sequencing Project, and an in-house database of 518 sequenced samples. Exome sequencing of both affected individuals of the Tunisian family was carried out by Macrogen on the Illumina HiSeq 1000 platform with Illumina TruSeq Exome Enrichment.

Tomography Analysis of Skeleton

Micro-computed tomography (CT) scans were performed with a μCT 50 system (SCANCO Medical) operated at 70 kV with a 0.5 mm Al filter and 500 ms exposure time per projection. 1,000 projections were captured over 180°. Images with 7.4 μm resolution were obtained after 3D data reconstruction. The images were downsized with a 0.5 scaling factor, and a 3D mean filter was applied to reduce noise. The segmentation was performed with a global threshold. The 3D rendering and the measurement were performed with Amira software (v6.3, FEI Visualization Sciences Group). After globally observing the entire skeleton, we assessed the volume of five skeleton pieces, the length of the left femur, and the shape of the cervical vertebrae.

Histology

Different mouse tissues were isolated at postnatal day 0 (P0), fixed in 10% neutral buffered formalin (Sigma-Aldrich, HT501128), and transferred into 70% ethanol before being embedded in paraffin and sectioned. Histological sections were stained with hematoxylin and eosin.

RT-PCR and qPCR

Total RNA was extracted with the NucleoSpin RNA kit according to the manufacturer's protocol (Macherey-Nagel, 740955). For each RT-PCR reaction, first-strand cDNA was generated from 1 μg of total RNA with the Maxima First Strand cDNA Synthesis Kit (Thermo Scientific, K1642). PCR amplification was carried out with the Maxima SYBR Green qPCR Master Mix (Fermentas, K0252) and the appropriate primer pair (Table S4). The reactions were monitored continuously in a Rotor-Gene thermal cycler (Corbett Research) according to the following program: 95°C for 10 min followed by 50 cycles of 95°C for 30 s, 55°C for 30 s, and 72°C for 30 s. All data were normalized to the expression levels of housekeeping genes *Eef2* (mouse) and *GAPDH* (human) according to the ($2^{-\Delta\Delta Ct}$) method.

Exon Trapping Assay

Cloning and Plasmid Preparation

Exons 7–11 of *CDK10* (GenBank: NM_052988) were cloned into the pET01 Exontrap vector from MoBiTec with primers flanked by restriction enzyme sites XhoI and BamHI (cdk10_pET01_XhoI_f and cdk10_pET01_BamHI_r, respectively). The vector and resulting PCR product were both digested with XhoI and BamHI (NEB), and the digested products were gel purified with the QIAquick Gel Extraction Kit (QIAGEN) and ligated with T4 DNA Ligase (Promega) overnight at 4°C. Resulting clones were verified by colony PCR with QIAGEN HotStarTaq Master Mix and primers pET01_cdk10_5r and pET01_cdk10_4f. Plasmids of two clones were purified with the EndoFree Plasmid Maxi Kit (QIAGEN), and the sequence was verified (see primers pENT01_cdk10_1/5-f/r in Table S4).

Cell Culture and Transfection

AD293 cells (Agilent) were transfected with 10 μg of plasmid DNA with the NEON Transfection System (Invitrogen) according to the following electroporation conditions: 1,100 V, 20 ms, and 2 pulse.

RNA Isolation and cDNA Screening

24 hr after transfection, cells were collected with 1 mL Trizol (Invitrogen), and RNA was isolated according to the manufacturer's protocol. cDNA was generated with the QuantiTech Reverse Transcription Kit (QIAGEN). For verification of the mutational impact on the splice donor site of exon 9, target cDNA was amplified with primers ETPR06 and ETPR07 from the Exontrap kit and analyzed by Sanger sequencing with ChromasLite software (Technelysium) and the UCSC Genome Browser.[16,17]

Homozygosity Mapping

Both affected individuals of the Tunisian family were genotyped on Affymetrix GeneChip Human Mapping 250K NspI arrays with dCHIP software[18] at the Center for Medical Research at the Medical University of Graz.

Generation of *Cdk10*^{flox} Mice and Other Transgenic Lines

The *Cdk10* mouse strain was generated essentially as described previously for *Cdk1*^{flox}.[19] Mouse genomic DNA harboring the *Cdk10* locus was isolated from the BAC clone pBACe3.6 RP23-297L8 (PKB983, Invitrogen). 5′ and 3′ retrieval homology arms were amplified by PCR (primers PKO1087 + PKO1091 for the 5′ arm and primers PKO1092 + PKO1093 for the 3′ arm) and subcloned into the pBlight-TK vector (PKB1009) according to the bacterial recombineering technique.[20] For generation of the targeting vector, the obtained pBlight-TK plasmid containing the entire *Cdk10* locus (PKB1015) was modified by the addition of a unique LoxP site in the intron downstream of exon 8 of *Cdk10* and a FRT-LoxP-eng2SA-Neo-FRT-LoxP cassette in the intron upstream of exon 2 of *Cdk10*. The resulting targeting vector (PKB1037) was linearized by PvuI digestion and introduced into embryonic stem (ES) cells by electroporation. After positive and negative selection with Geneticin and ganciclovir, respectively, genomic DNA of surviving ES cell colonies was screened for homologous recombination by Southern hybridization using 5′ (290 bp) and 3′ (323 bp) external probes generated by PCR from BAC DNA with the use of primer pairs PKO1046 + PKO1047 and PKO1048 + PKO1049, respectively. Digest with restriction enzymes EcoRV and NotI and hybridization with the 5′ probe characterized clones that carried the wild-type (WT) band at 15.8 kb and the targeted band at 6.2 kb. Digest with NheI and hybridization with the 3′ probe resulted in clones that carried the WT band at 14.3 kb and the targeted band at 6.1 kb. Three correctly targeted ES cell clones (4021, 4023, and 4032) were selected for microinjection into blastocysts and derivation of chimeric mice for the generation of the *Cdk10*-conditional-knockout mouse strain.

Obtained mice carrying the eng2SA-neomycin cassette (*Cdk10*$^{+/neo}$) were bred with β-actin-Flpe transgenic mice[21] (strain B6.Cg-Tg(ACTFLPe) 9205Dym/J; stock no. 005703; the Jackson Laboratory) for the removal of the eng2SA-neomycin cassette and generation of the *Cdk10*^{flox} allele. The *Cdk10*^{null} allele, in which the deletion of exons 2–8 creates a frameshift, was the result of crossing *Cdk10*$^{+/neo}$ mice with β-actin-Cre transgenic mice[22] (strain FVB/N-Tg(ACTB-cre)2Mrt/J; stock no. 003376; the Jackson Laboratory). Mice were housed under standard conditions with food and water available *ad libitum* and maintained on a 12 hr light-dark cycle. Mice were fed a standard chow diet containing 6% crude fat and were treated humanely in compliance with the guidelines of the institutional animal care and use committee at the Biological Resource Center (BRC) at Biopolis, Singapore.

Genotyping

For genotyping PCR of *Cdk10* WT, flox, and null alleles, primers Pr1 (PKO1229), Pr2 (PKO2647), and Pr3 (PKO2648) (Table S4) were used at 1 μM final concentration. In brief, cells or tissue pieces to be genotyped were lysed by being boiled in lysis solution (25 mM NaOH [pH 12] and 0.2 mM EDTA) for 20–30 min for the extraction of genomic DNA.[23] Alkaline pH was neutralized by the addition of an equal volume of neutralization buffer (40 mM Tris-HCl [pH 5]). 1 μL of the resultant genomic DNA solution was used as a template in 20 μL of PCR reaction with 0.5 units of DreamTaq polymerase (Bioline). 30 PCR cycles with 30 s denaturation at 94°C and 1 min annealing and extension at 62°C were performed for amplification of different alleles of *Cdk10*, resulting in a band of 283 bp (*Cdk10*^{WT}), 398 bp (*Cdk10*^{flox}), or 508 bp (*Cdk10*^{null}).

Gene Expression Analysis

For microarray analysis, RNA from mouse tissue (kidney, lung, heart, brain, stomach, intestine, thymus, and liver) was isolated with the Invitrogen PureLink RNA Mini Kit. RNA was prepared with the Illumina TotalPrep RNA Amplification Kit according to the manufacturer's protocol. The raw Illumina MouseRef-8 v2.0 Expression BeadChip array data were subjected to quality-control inspection, during which probes were removed for the following reasons: the probe quality was bad, the probe had no match, probe sequence was not from chromosomes 1–19, or the gene represented by the probe was not found in Entrez or Ensembl. The data intensity was not further normalized given that the gene expression levels were highly consistent within each organ (between the knockout and the heterozygous control). The expression data were converted into a ratio between the knockout and the control in each organ and $\log_2$ transformed for statistical analysis. A model-based method called EBprot[24] was applied to ratio data from each organ and reported the posterior probability of differential expression and associated false-discovery rate (FDR). A gene was considered to be differentially expressed if it was statistically significantly different in at least two organs (FDR 1% and minimal fold change 50%). Enrichment of biological functions, represented by Gene Ontology and CPDB,[25] was evaluated with an in-house implementation of a hypergeometric test.

Isolation and Culture of Primary Mouse Embryonic Fibroblasts

Primary mouse embryonic fibroblasts (MEFs) of WT (*Cdk10*$^{+/+}$) and knockout (*Cdk10*$^{-/-}$) genotypes were isolated from embryonic day 13.5 (E13.5) mouse embryos as described previously.[19] In brief, the head and the visceral organs were removed, the embryonic tissue was chopped into fine pieces with a razor blade and trypsinized for 15 min at 37°C, and finally tissue and cell clumps were dissociated by pipetting. Cells were plated in a 10 cm culture dish (passage 0) and grown in HyClone high-glucose DMEM (GE Healthcare, SH30243) supplemented with 10% fetal bovine serum (GIBCO, 26140) and 1% penicillin-streptomycin (Invitrogen, 15140-122). Primary *Cdk10*$^{+/+}$ and *Cdk10*$^{-/-}$ MEFs were immortalized by serial passaging 30 times according to a modified 3T3 protocol.[26]

Primary human dermal fibroblasts were isolated from fresh skin biopsies obtained from subject 6 and an ethnically matched healthy control individual. Fibroblasts were cultured in high-glucose DMEM supplemented with 1% L-glutamine, 10% fetal bovine serum, and 1% penicillin-streptomycin. Both primary and immortalized MEFs and human fibroblasts were cultured in a humidified incubator with 5% CO_2 and 3% O_2.

Proliferation Assay and FACS Analysis

For alamarBlue proliferation assays, 1,500 cells in a volume of 150 μL were plated per well of 96-well plates in 6 replicates for each clone. Starting 24 hr after seeding, cells were incubated for 4 hr in a final volume of 300 μL after the addition of 150 μL

of assay medium (1:5 ratio of alamarBlue [AbD Serotec, BUF012B] to growth medium), and metabolic activity was quantified via measurement of the fluorescence at 585 nm.

For BrdU labeling and fluorescence-activated cell sorting (FACS) analysis, primary MEFs serum starved for 72 hr were trypsinized and replated in 10 cm dishes with DMEM supplemented with 10% fetal bovine serum for the induction of synchronized entry into the cell cycle. For monitoring S phase, cells were labeled with 100 μM BrdU (BD PharMingen, 550891) for 1 hr before being collected at different time points. At the end of each time point, cells were trypsinized and fixed in −20°C 70% ethanol and stained with anti-BrdU antibodies (BD PharMingen, 555627) followed by Alexa-Fluor-647-labeled goat-anti-mouse secondary antibodies (Invitrogen, A21235). Cells were counterstained for DNA content with propidium iodide (Sigma, 81845). Cell-cycle analysis was performed by FACS on a LSRII cytometer (BD Biosciences), and the resulting data were analyzed by FlowJo 8 software.

Cell Lysis, SDS-PAGE, and Immunodetection

Cells were lysed in Laemmli buffer (60 mM Tris-HCl [pH 6.8], 10% glycerol, 100 mM DTT, and 2% SDS) and supplemented with protease inhibitors (10 μg/mL each of leupeptin, chymostatin, and pepstatin [Chemicon EI8, EI6, and EI10, respectively]). 10 or 20 μg of protein extracts was separated on 9% or 8% polyacrylamide gels, transferred onto polyvinylidene difluoride membranes (Millipore, IPVH0010) with a semi-dry system, and blocked in Tris-buffered saline with 0.1% Tween 20 and 4% non-fat dry milk (Bio-Rad, 1706404). Blots were probed with the appropriate primary antibodies overnight at 4°C and subsequently with secondary goat-anti-mouse (Pierce, 0031432) or anti-rabbit antibodies (Pierce, 0031462) conjugated to horseradish peroxidase and were developed with an enhanced chemiluminescence reagent (PerkinElmer, NEL105001EA). The antibodies used were cyclin A2 (Santa Cruz, SC-596), total pRB (BD-PharMingen, 554136), HSP90 (BD-Transduction Laboratories, 610419), and Ets2 (Santa Cruz, SC351).

Generation of Antibodies against CDK10

Two peptide sequences corresponding to the C terminus (HHRNKRAAPAAAEGQSKRC) and T-loop (CIMLQVLRGLQYLHR) of CDK10 were synthesized by Keck Biotechnology Resource Laboratory and GL Biochem (Shanghai), respectively. The sequences were then coupled to mcKLH as previously described.[27] 1 mg of mcKLH-conjugated peptides was mixed with Freud's complete adjuvant and injected subcutaneously into two rabbits on day 0. All subsequent immunizations on days 14, 35, 56, 77, 98, 119, 140, 161, 182, 203, 224, 245, and 266 were in the presence of Freud's incomplete adjuvant. Rabbits were bled on days 0, 49, 70, 91, 112, 133, 154, 175, 196, 217, 238, 259, and 280, and sera were stored at –80°C. Serum from Blk319R was subsequently affinity purified through a column covalently coupled to both peptides, and it was then concentrated. All purified antibodies were reconstituted to a final concentration of 1 mg/mL in PBS and 50% glycerol and were stored at –20°C.

Immunofluorescence Microscopy

Cells were grown on coverslips (Lab Tek) before serum starvation. At different time points, cells were fixed with 4% PFA for 10 min. The fixed cells were permeabilized for 10 min with 0.2% Triton X-100 and exposed to a blocking solution over the course of 1 hr (PBS, 0.2% Triton X-100, and 2% BSA [Sigma]). Cells were stained with primary antibodies directed against Arl13B (ProteinTech Group, 17711-1-AP) and gamma-tubulin (Sigma-Aldrich, T6557) for 1 hr at room temperature and then incubated with Alexa-Fluor-488-labeled goat-anti-mouse (Invitrogen, A11029) and Alexa-Fluor-555-labeled goat-anti-rabbit (Invitrogen, A21428) secondary antibodies for 1 hr. Cells were counterstained with DAPI. Images were acquired at 100× magnification on an Olympus FluoView upright laser scanning confocal microscope. 15 confocal images of cilia were randomly captured for each experiment. Ciliary length of the longest cilium in each confocal image was analyzed with Olympus FluoView FV1000 v3.1 software. Statistical analysis was done with GraphPad Prism and a Student's t test, and the average ciliary length was calculated.

Results

We report here the clinical, genetic, and molecular etiology of a syndrome that was independently uncovered by five research teams and investigated collaboratively with the use of GeneMatcher.[28] The investigations were performed in accordance with the ethical standards of the responsible committee on human experimentation. Parents of all affected individuals provided written informed consent for genetic analyses of their affected children and themselves in accordance with the ethical standards of the institutional review boards.

CDK10 Mutations Cause a Growth-Retardation Syndrome

We have identified nine individuals with homozygous mutations in *CDK10* from five unrelated families (Figure 1A). The detailed description of the clinical features can be found in the Supplemental Note, Table 1, and Table S1.

Seven boys and two girls originating from Turkey, Algeria, Tunisia, or Saudi Arabia were found to have a mean height of −3 SD (range: −1.3 to −4.5 SD), mean weight of −3.1 SD (range: −0.2 to −4.7 SD), and mean occipitofrontal circumference of −2.2 SD (range: −4.6 to +3 SD). They all displayed developmental delays, a mean age of sitting of 19 months (range: 11–30 months), a mean age of walking of 33 months (range: 22–48 months), and a pronounced language delay. The estimated degree of intellectual disability was moderate to severe, and all displayed a learning disorder. They shared dysmorphic facial features: a triangular face with a small pointed chin, low-set and posteriorly rotated ears, a depressed or wide nasal bridge with a broad nasal tip, telecanthus, and epicanthal folds. Orthopaedic anomalies included joint hyperlaxity and pes planus. A sacral dimple was observed in five of seven affected individuals. Brain MRI indicated hypoplasia of the corpus callosum in three individuals (Figure 1B, Table 1, and Table S1). A skeletal survey uncovered that all but one investigated individual had striking cervical spine anomalies, including clefting of the posterior arch of the atlas (C1) and partial fusion of C2 and C3 cervical vertebrae (Figures 1D–1F). The spine abnormalities are a hallmark of this syndrome.

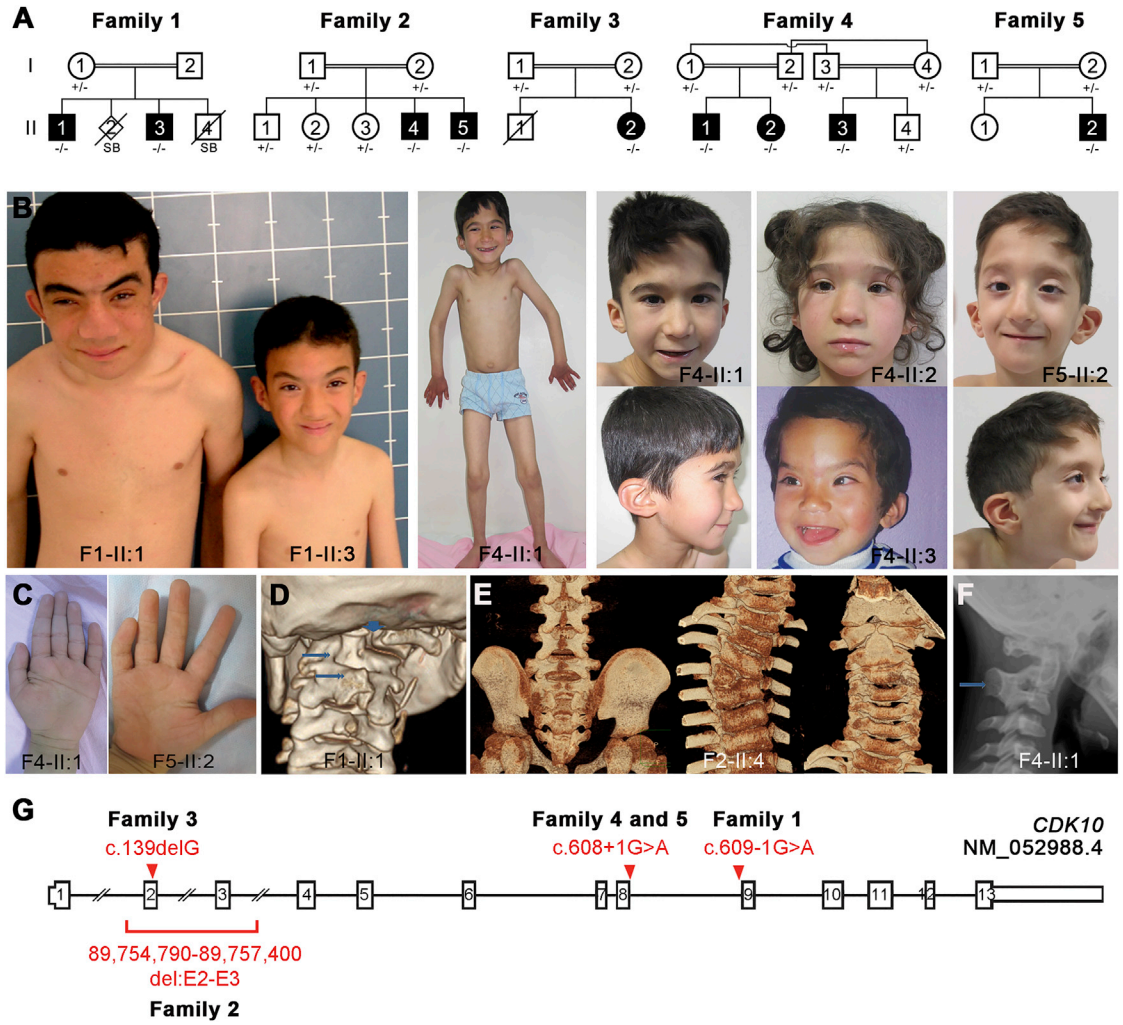

Figure 1. Biallelic Germline Mutations in *CDK10* in Nine Individuals from Five Consanguineous Families
(A) Pedigrees of families from Tunisia (1), Algeria (2), Saudi Arabia (3), and Turkey (4 and 5). The affected individuals carry homozygous germline mutations in *CDK10*. Open symbols represent unaffected individuals, and filled symbols represent affected individuals.
(B) Photographs of affected individuals show facial dysmorphisms.
(C) Hand anomalies with clinodactyly of the fifth finger and single transverse palmar crease.
(D) Severe mal-segmentation of the cervical vertebrae in proband F1-II:1.
(E) Lack of fusion of the posterior arches of S2–S5, right T4 hemivertebrae, and lack of fusion of the anterior arch of the atlas and partial fusion of C2 and C3 vertebrae in proband F2-II:4.
(F) Fusion of the cervical vertebrae in proband F4-II:1.
(G) Exon-intron structure of *CDK10* on chromosome 16 shows the position of the four identified homozygous mutations.

A combination of array CGH, SNP-array-based whole-genome homozygosity mapping, and whole-exome sequencing in these five families revealed a common genetic etiology consisting of distinct germline *CDK10* homozygous mutations. The intron 8 splice-acceptor-site mutation c.609−1G>A (GenBank: NM_052988.4) segregated in family 1, the single-nucleotide deletion c.139delG (p.Glu47ArgfsTer21) segregated in family 3, the splice-donor-site mutation c.608+1G>A segregated in families 4 and 5, and a small (2.6–28 kb) homozygous 16q24.3 microdeletion encompassing exons 2 and 3 of *CDK10* segregated in family 2 (Figures 1A and 1G and Figure S1). We suggest naming this previously unrecognized congenital disease with *CDK10* mutations as Al Kaissi syndrome.

CDK10 Splice-Site Mutations Behave as Loss-of-Function Alleles

Four differentially spliced transcripts expressed from the *CDK10* locus were previously described[29,30] (Figure S1). These transcripts differ in their 5′ and 3′ UTRs and in exon 11. Most likely only two of these transcripts are functional: the full-length transcript (GenBank: NM_052988.4), which encodes the 360 amino acid CDK10 kinase; and a shorter transcript (GenBank: NM_052987.3), which encodes a truncated 272 amino acid CDK10 variant. The latter is missing the ATP-binding domain and therefore encodes most likely a catalytically inactive form of CDK10.

To test whether splicing of the endogenous *CDK10* transcripts is affected in family 4, we grew and compared

Table 1. Clinical Features of Nine Individuals with *CDK10* Mutations

	Family 1		Family 2		Family 3	Family 4			Family 5
***CDK10* Mutation**									
Genomic position (hg19)	chr16: 89,760,580 G>A		arr 16q24.3 89,754,790 −89, 757,400 × 0		chr16: 89,755, 711delG	chr16: 89,759,876 G>A	chr16: 89,759,876 G>A	chr16: 89,759,876 G>A	chr16: 89,759,876 G>A
cDNA change	c.609−1G>A		ND	ND	c.139delG	c.608+1G>A	c.608+1G>A	c.608+1G>A	c.608+1G>A
Demographic Data									
Individual (year of birth)	individual 1 (1997)	individual 2 (2002)	individual 3 (2009)	individual 4 (2011)	individual 5 (2013)	individual 6 (2008)	individual 7 (2010)	individual 8 (2013)	individual 9 (2008)
Sex	male	male	male	male	female	male	female	male	male
Individual ID	F1-II:1	F1-II:3	F2-II:4	F2-II:5	F3-II:2	F4-II:1	F4-II:2	F4-II:3	F5-II:2
Ancestry	Tunisian	Tunisian	Algerian	Algerian	Saudi Arabian	Kurdish (from Turkey)	Kurdish (from Turkey)	Kurdish (from Turkey)	Turkish
Consanguinity	+	+	+	+	+	+	+	+	−
Growth Parameters									
Age at examination	9 years	4 years	7 years 8 months	4 years 11 months	18 months	8 years 11 months	7 years 3 months	3 years 9 months	6 years 8 months
Height (SD)	114 cm (−3)	93 cm (−2.5)	111.8 cm (−2.5)	96 cm (−3)	75 cm (−1.3)	106 cm (−4.4)	97.5 cm (−4.7)	86 cm (−3.5)	107 cm (−2.6)
Weight (SD)	17 kg (−3)	11.75 kg (−3)	16.2 kg (−2.9)	12.3 kg (−3.2)	8.4 kg (−0.2)	12.2 kg (−4.7)	11.5 kg (−4.2)	10.5 kg (−3.4)	13.5 kg (−3)
Occipital frontal circumference (SD)	50 cm (−2.3)	47 cm (−3)	51.5 cm (−0.8)	49 cm (−2)	50 cm (3)	46.5 cm (−4.6)	46 cm (−4.4)	44 cm (−3.9)	49.5 cm (−2)
Developmental Stages									
Age of sitting (months)	17	15	18	18	30	18	20	24	11
Age of walking (months)	24	22	30	48	cannot walk	42	35	40	24
Language skills	severely mentally impaired	severely mentally impaired	two-word combinations, no sentence	no words	two-word combinations, no sentence	simple two-word sentences, 40–50 words	compatible with 3 years of age	simple words, no word combinations	no sentences, two-word combinations
Cognitive Skills									
Learning disorders	+	+	+	+	+	+	+	+	+
Estimated degree of ID	moderate to severe	moderate to severe	moderate to severe	moderate to severe	severe	moderate to severe	moderate to severe	moderate to severe	moderate to severe
Dysmorphic Features									
Telecanthus	+	+	+	+	−	−	+	+	+
Bilateral epicanthal folds	+	+	+	+	+	+	+	+	+
Downslanting palpebral fissures	+	+	+	+	−	−	−	−	−

(*Continued on next page*)

Table 1. *Continued*

	Family 1		Family 2		Family 3	Family 4		Family 5	
Depressed nasal bridge	+	+	+	+	+	wide	wide	+	wide
Broad nasal tip	+	+	+	+	+	+	+	+	+
Long philtrum	+	+	+	+	+	+, smooth	+, smooth	+, smooth	+, smooth
Small chin	+	+	+	+	+	–	–	–	–
Triangular face	+	+	+	+	–	–	–	–	–
Low-set ears	+	+	+	+	+	+	+	+	+
Posteriorly rotated ears	+	+	+	+	+	+	+	+	+
Other	macrodontia	macrodontia	nevus flammeus of the glabellar region	nevus flammeus of the glabellar region	high-arched palate, brachycephaly, synophrys	malar rash, high-arched palate, pointed chin	malar rash, high-arched palate, pointed chin	nevus flammeus of the glabella, malar rash	strabismus, malar hypoplasia, high-arched palate
Hand Examination									
Small hands	+	+	+	+	–	+	+	+	+
Deep palmar creases	+	+	+	+	–	–, bilateral single transverse palmar crease	–	–	–

primary skin fibroblasts from proband II:1 with ethnically, age-, and sex-matched dermal fibroblasts from a healthy donor. Using primers spanning exons 7–10, we detected a shorter amplicon in the proband's cells than in control cells (Figure 2A). WT and mutant amplicons were gel extracted for cloning, and multiple clones were sequenced. Several aberrant splice isoforms were identified: MUT1 skipped exon 8, MUT2 skipped exons 8 and 10, and MUT3 skipped exon 8 and retained intron 9 (Figure 2B). Compared with the longest *CDK10* transcript (GenBank: NM_052988.4), each of these mis-spliced transcripts can result in truncated mRNAs (Figure 2B). Given that RNA samples were not available for family 1, we used an exon trap vector system (pET01, MoBiTec GmbH, Göttingen, Germany) to address the consequences of the mutation on the cDNA level. Sequencing of the resulting transcripts revealed exon 9 skipping, which presumably leads to the in-frame deletion p.Tyr204_Trp223del (Figure 2B). In conclusion, all mutant transcripts resulted in frameshifts or internal truncations, establishing the deleterious effect of the donor c.608+1G>A and acceptor c.609−1G>A splice-site mutations in intron 8.

Using a series of primers covering the *CDK10* cDNA, qPCR revealed significantly reduced overall *CDK10* levels, suggestive of nonsense-mediated decay of mutant transcripts (Figure 2C). The levels of ETS2, which is phosphorylated by CDK10 and subsequently targeted for degradation,[4] were increased (Figure 2D), consistent with absent or reduced CDK10 kinase activity in subject-derived cells. Despite these changes, mutant and WT cells did not exhibit differential growth parameters (Figure 2E) when grown in complete (10% serum) media over 7 days. Together, these results indicate that the classical splice-site mutations uncovered here behave like loss-of-function *CDK10* alleles, which do not impair cell growth *ex vivo* but cause a severe growth retardation syndrome during human development.

Cdk10-Knockout Mice as a Model for Al Kaissi Syndrome

To better understand the requirement for CDK10 at the tissue and organismal levels, we generated a complete knockout of the homologous *Cdk10* in mice. We accomplished this by deleting exons 2–8 of *Cdk10* via standard recombineering techniques (Figure S2A). Recombination at the correct locus was verified by Southern blotting, genotyping, and qPCR analysis (Figures S2B–S2D). Even though homozygous *Cdk10* mutants (*Cdk*10KO) were detected at a normal Mendelian ratio on E17.5, fewer than 6% of the embryos were born, indicating partial prenatal lethality (Figure 3A). Of the *Cdk10*KO mice born, very few survived the first day of life, suggesting that *Cdk10* is an essential gene during mouse development. Similar to the individuals with *CDK10* mutations (see Figure 1), all *Cdk10*KO embryos and mice displayed severe growth retardation (Figures 3B and 3C). The combination of growth retardation and lethality suggests that *CDK10* is an essential gene like a number of other

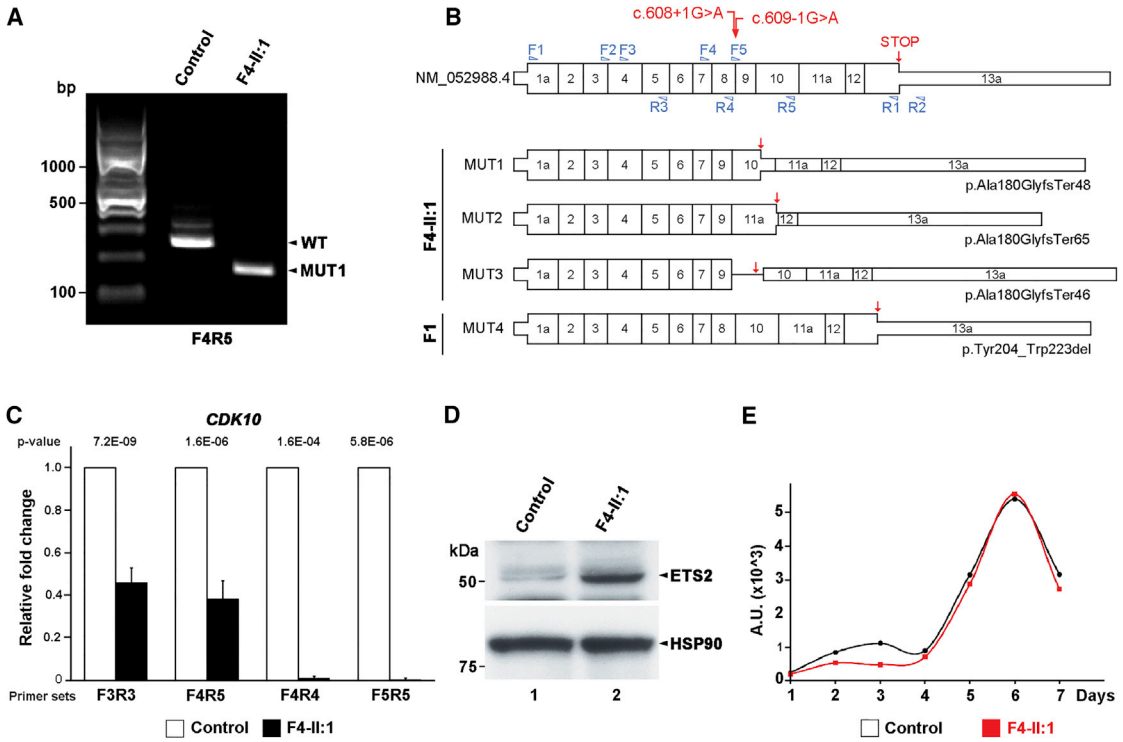

Figure 2. *CDK10* Splice-Site Mutations Reduce Endogenous mRNA Levels and Increase ETS2 Levels
(A) RT-PCR performed on primary dermal fibroblasts derived from affected (F4-II:1) and control individuals indicates aberrant splicing of endogenous *CDK10* mRNA.
(B) Schematic representations of the wild-type *CDK10* isoform and four mutant transcripts cloned from primary fibroblasts with intron 8 donor and acceptor splice-site mutations.
(C) qRT-PCR analysis demonstrates lower endogenous *CDK10* mRNA levels in cells derived from affected individuals than in control cells, suggestive of nonsense-mediated decay.
(D) Whole-cell lysates of human fibroblasts from control and affected individuals were separated on SDS-PAGE, and immunoblots were stained with antibodies against ETS2 and HSP90. Cells with reduced or absent CDK10 kinase activity displayed increased levels of ETS2, which is normally degraded once it is phosphorylated by CDK10.
(E) Primary human fibroblasts from control and affected individuals were grown in the presence of serum over 7 days and did not show any noticeable differences.

cell-cycle regulatory genes, including *CDK1* (MIM: 116940)[19] and *MASTL* (MIM: 608221).[31] Therefore, we isolated MEFs from *Cdk10*KO and WT embryos on E13.5 to analyze their cell-cycle and proliferation characteristics. Surprisingly, the proliferation rate, cell-cycle progression determined by FACS, and timely expression of cyclin A2 and phosphorylated retinoblastoma protein (Rb) were indistinguishable between WT and *Cdk10*KO MEFs (Figure S5), indicating that CDK10 is not essential for cellular proliferation. We hypothetize that the growth retardation in *Cdk10*KO embryos is more likely driven by developmental defects rather than a strictly cell-autonomous requirement of CDK10.

Because individuals with *CDK10* mutations display unique skeletal defects, we analyzed newborn *Cdk10*KO pups by using micro-CT (Figure 3D). We observed several bone defects that affect the axial skeleton, including a reduced volume of mineralized matrix from the head, the occurrence of bifidity (clefting) at C1 (atlas) or C2 (axis), and the absence of dens (Figure 3D and 3E and Figures S3 and S4). The appendicular skeletal defects are characterized by the volume reduction of mineralized matrix from the femur, tibia, and fibula, the length reduction of the left femur, and the malformations of the mandible (Figure S3). Therefore, the *Cdk10*KO mouse model partly recapitulates the phenotype observed in individuals with loss-of-function *CDK10* mutations.

Mice with Mutant *Cdk10* Display Defects in Multiple Organs

In addition to observing growth retardation, we detected defects in several organs of the *Cdk10*KO mice, including in the kidney, lung, heart, spleen, liver, and muscle (Figure S6). For example, *Cdk10*KO mouse kidneys displayed severe tubulonephrosis. Approximately 30%–50% of available renal tubules were severely degenerated or necrotic. Most of the affected tubules were lined with severely attenuated mineralized epithelium, and their lumens contained mineralized casts. Other tubules were lined with swollen and vacuolated epithelium that occasionally displayed nuclear pyknosis (indicative of necrosis). In *Cdk10*KO lungs, most of the alveoli and bronchioli

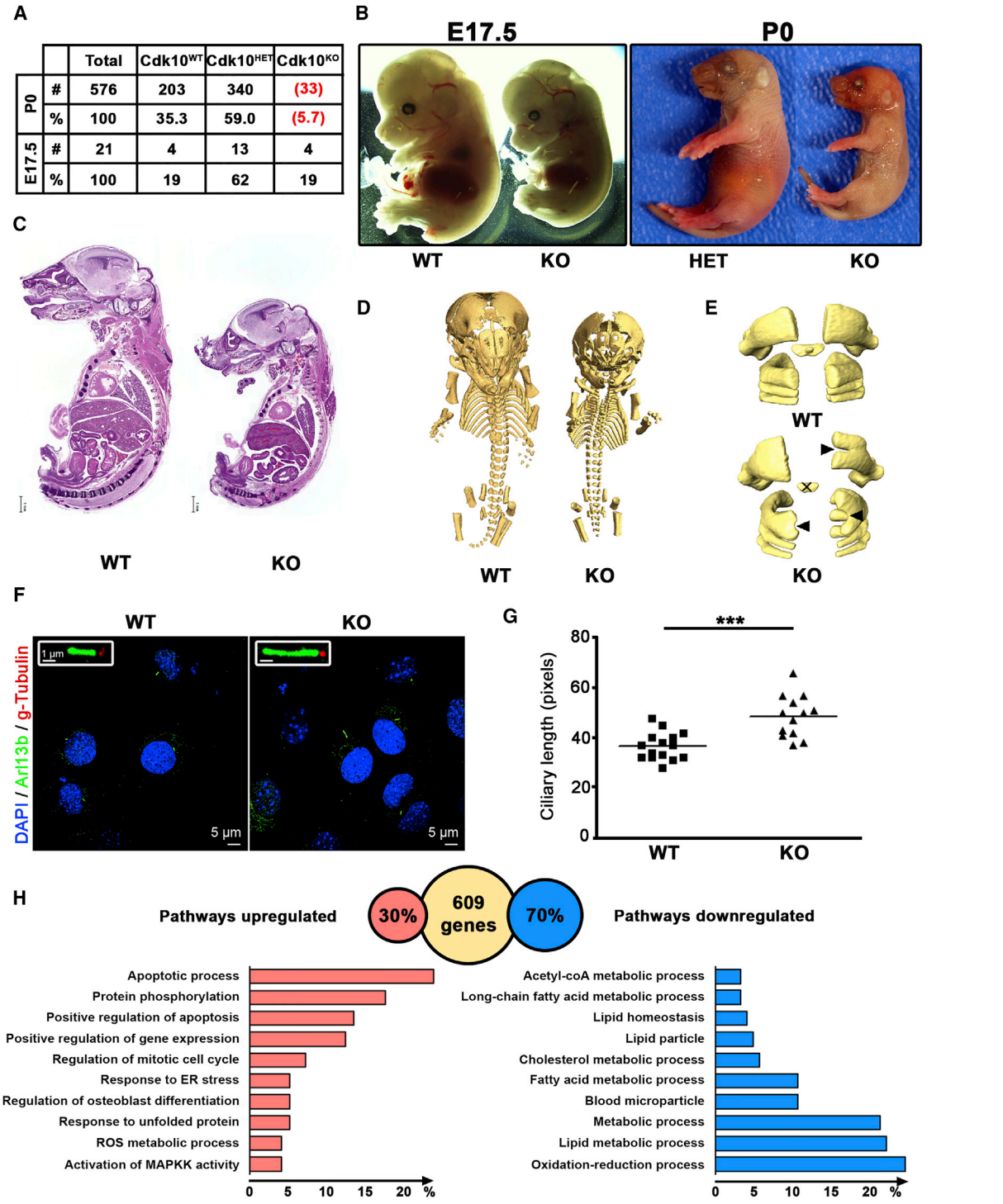

Figure 3. Mice Lacking *Cdk10* as a Model for the Human Disease

(A) Heterozygous *Cdk10*$^{WT/KO}$ mice were interbred, and the genotypes of the offspring were analyzed at embryonic day 17.5 (E17.5) and birth (P0). Numbers in red indicate that pups were dead at the moment of collection.

(B) Control *Cdk10*$^{WT/WT}$ (WT), heterozygous *Cdk10*$^{WT/KO}$ (HET), and knockout *Cdk10*$^{KO/KO}$ (KO) embryos at E17.5 and pups at P0 were isolated and photographed.

(C) Hematoxylin & eosin staining of sagittal sections of the entire *Cdk10*$^{WT/KO}$ and *Cdk10*$^{KO/KO}$ P0 pups. The scale bar represents 1 mm.

(D) 3D µCT images of the mineralized part of the entire skeleton from *Cdk10*$^{WT/WT}$ and *Cdk10*$^{KO/KO}$ P0 pups. Note the shorter stature of the *Cdk10*KO pups and the defects in the vertebrae.

(E) 3D µCT images of C1–C4 vertebrae from *Cdk10*$^{WT/WT}$ and *Cdk10*$^{KO/KO}$ P0 mice. Note the presence of bifidity (black arrow) and the absence of mineralized dens (cross) in the *Cdk10*$^{KO/KO}$ mice.

(F) *Cdk10*KO and WT MEFs were starved for 4 days, and cilia were stained with Arl13b and gamma-tubulin antibodies. The inset shows magnified cilia.

(legend continued on next page)

were collapsed and failed to open (fetal atelectasis). The interalveolar septae were markedly thickened and were composed of collapsed alveolar walls and few lymphocytes and macrophages. The few inflated (opened) alveoli had squamous debris and activated foamy macrophages in their lumens. The bronchioles were partially filled with eosinophilic fluid and squamous debris. The current pulmonary atelectasis (failure of lung to inflate at birth) was severe and was the likely cause of death of the homozygous *Cdk10*KO mice. The cardiac and renal lesions might also have contributed to the general weakness and demise of these mutant mice. Diffuse fetal atelectasis usually leads to severe hypoxia and death. Causes of fetal atelectasis include weakness of respiratory diaphragmatic and intercostal muscles, which can lead to insufficient respiration attempts at birth, bronchial obstruction, or absence of alveolar surfactant.

Organs with Mutant *Cdk10* Show Defects in Metabolic and Cilia-Related Genes

Because the phenotype of the *Cdk10*KO mice and individuals with *CDK10* mutations is multifaceted and affects multiple organs, we carried out unbiased gene expression analysis on eight different organs (kidney, lung, heart, brain, stomach, intestine, thymus, and liver) from WT and *Cdk10*KO mice (Figure 3H and Figure S7). A total of 609 transcripts, including *Cdk10* as expected (Figures S7A–S7C and Table S2), were differentially expressed in at least two different organs. Approximately 70% of the genes were downregulated (Figure 3H), indicating that CDK10 directly or indirectly stimulates gene expression. Pathway analysis indicated that 175 metabolic genes were enriched (Table S3). Of the 175 metabolic genes differentially regulated, lipid metabolic processes involving *HMGCS2* (MIM: 600234), *LIPO1* (MIM: 613921), and *LIPA* (MIM: 613497) stood out (Figure S7C and Table S3). HMGCS2 is a mitochondrial enzyme that catalyzes the first and rate-limiting reaction of ketogenesis, an important process that allows alternative metabolic adaptation by using lipids as energy sources in starved cells (for a review, see Puchalska and Crawford[32]). *Hmgcs2* was almost 20-fold upregulated in WT MEFs upon serum starvation, whereas *Hmgcs2* expression remained unchanged in *Cdk10*KO cells (Figure S7D). These data suggest that a metabolic impairment might contribute to the stunted growth of mice and humans with *Cdk10* mutations.

As expected, a mild upregulation of *Ets2* expression was detected upon CDK10 depletion (Figure S7D). CDK10 is activated by cyclin M and interacts with ETS2.[6,7] To confirm the increase in ETS2 at the protein level, we performed western blots with lysates of subject-derived primary fibroblasts (see Figure 2D). The levels of ETS2 were substantially higher in CDK10 mutant cells than in control cells, which is in accordance with the finding that ETS2 is a substrate of the CDK10/cyclin M complex.[7]

Finally, expression levels of genes involved in ciliogenesis, including *BBS4* (MIM: 600374), *CEP290* (MIM: 610142), and *RPGRIP1L* (MIM: 610937) (Figure S7D), differed between organs with mutant CDK10 and control organs. Mutations in these genes can lead to ciliopathies such as Bardet-Biedl syndrome (MIM: 615982) or Joubert syndrome (type 5 [MIM: 610188] or type 7 [MIM: 611560]). To investigate the functional consequences of differential expression of cilia-related genes, we examined cilia growth and length in serum-starved *Cdk10*KO MEFs. Immunostaining, using ARL13B and gamma-tubulin antibodies, revealed significantly longer cilia in *Cdk10*KO MEFs than in WT cells (Figures 3F and 3G), corroborating results that were reported after the silencing of *Cdk10* or cyclin M by siRNA[10] (for a review, see Guen et al.[33]). BBS4, which interacts with CEP290,[34] is a BBSome component that is essential for cilia formation,[35] providing a rationale for our observation of longer cilia in *Cdk10*KO MEFs.

Discussion

Our work has uncovered nine individuals with germline recessive mutations in *CDK10*. The clinical features of these individuals display little phenotypic variability and are best summarized by severe growth retardation, spine malformations, facial dysmorphisms, developmental delays, and intellectual disability (see Figure 1, Table 1, and Table S1).

Because cyclin M binds to and activates CDK10, and mutations in *FAM58A* (the gene encoding cyclin M) lead to STAR syndrome (MIM: 300707),[8,9] we compared the two syndromes (see Table S5). Superficially, the two syndromes might appear related, but careful comparison reveals that they are clinically distinct. The spine malformations, developmental delays, and intellectual disability are important symptoms present in this syndrome but absent from STAR syndrome. In addition, the severity of the growth retardation is more pronounced in individuals harboring *CDK10* mutations. Distinctive features of STAR syndrome, such as toe syndactyly and anogenital, renal, and urinary-tract malformation, are rarely found in the syndrome described here. Given that we observed incomplete clinical overlap between STAR and Al Kaissi syndromes, we hypothesize either that the nature of the mutation is different or that CDK10 has additional binding

(G) Quantification of the maximal length of the cilia in WT and *Cdk10*KO MEFs. ***p value < 0.001 (Student's t test).
(H) Pathway analysis from gene expression data of eight different tissues obtained from $Cdk10^{WT/WT}$ and $Cdk10^{KO/KO}$ P0 mice. From the entire dataset, 609 genes were differentially expressed in at least two tissues. In the absence of *Cdk10*, 30% of these genes were downregulated and 70% were upregulated. Pathway analysis for datasets of up- and downregulated genes is displayed as the percentage of genes annotated for the indicated pathway.

partners beyond cyclin M. The phenotype in the *Cdk10*KO mice is similar in terms of growth retardation and spine malformation, whereas other aspects have not been examined yet. The analysis of the *Cdk10*KO brain warrants further investigation in light of the observed intellectual ability of individuals with *CDK10* mutations. In addition, *Cdk10*KO newborn pups displayed a number of phenotypes that have not been detected yet in individuals with *CDK10* mutations. They include lung defects, kidney problems, and others. Several reasons could explain the differences observed between mice and humans: (1) all *Cdk10* transcripts are lost in the mutant mice, whereas in humans only a subset of them might carry a mutation, (2) some defects might not have been documented yet in the individuals with *CDK10* mutations as a result of differential disease progression, or (3) the requirement or genetic compensations in mice could be different in humans.

CDK10 has been shown to interact with the transcription factor ETS2 and to affect its transactivation activity.[6] CDK10/cyclin M complexes phosphorylate ETS2 on several residues to control its half-life, and ETS2 was the first direct CDK10 substrate to be identified. In our experiments, we uncovered that in the absence of CDK10, endogenous ETS2 was present at higher levels, which confirms previous reports. This result is noteworthy given that overexpression of ETS2 has been observed in Down syndrome (MIM: 190685), and overexpression of *Ets2* in mice leads to skeletal abnormalities that are comparable to those of *Cdk10*KO mice and individuals harboring *CDK10* mutations.[36] These data indicate that the spine malformations observed in individuals with *CDK10* mutations and in *Cdk10*KO mice could be a direct consequence of elevated ETS2 levels, suggesting that inhibition of ETS2 activity could potentially reduce the severity of spine malformations in affected individuals.

Among the most surprising results from our study is the effect of CDK10 on the expression of genes involved in lipid metabolism. Our unbiased transcriptomic approach revealed across multiple organs that approximately one-third of differentially expressed genes were involved in metabolism. Among these, *HMGCS2* is particularly interesting because of its function in ketogenesis.[32] Likewise, *LIPA* and *LIPJ* might function in the same pathway. We have confirmed the differential expression of these genes in subject-derived dermal fibroblasts (see Figure S7E). Although we have not been able to document overtly altered lipid profiles in individuals with *CDK10* mutations, it will be very important to perform a thorough metabolic phenotyping of these probands to document whether their diet might offer a therapeutic window for mitigating their severe growth retardation.

Silencing of *CDK10* in cell lines was reported to lead to longer cilia,[10] and indeed we detected altered expression of a number of genes involved in ciliogenesis (*BBS4*, *CEP290*, and *RPGRIP1l*; see Figure S7E) in mutant cells from affected individuals. Although there is no clinical resemblance between Al Kaissi syndrome and Bardet-Biedl syndrome, we detected that monocilia are longer in *Cdk10*KO MEFs. Together with the lung histology of *Cdk10*KO mice and the recurrent infections seen in individuals with *CDK10* mutations, this suggests that ciliary defects might contribute to the phenotype of individuals with *CDK10* mutations. Although our results indicate that CDK10 does not affect the proliferation capacity of primary fibroblasts, we cannot rule out that other cell types would be differentially affected. It is clear that loss of CDK10 is detrimental during embryonic stages but not necessarily after development is complete. In line with this, we observed that knockout of *Cdk10* in adult mice (C$dk10^{flox/flox}$ ROSA26-CreERT2 treated with tamoxifen) had little to no effect (data not shown). Therefore, future studies will need to address whether loss of CDK10 affects proliferation during development. Alternatively, loss of CDK10 could affect differentiation, which would also result in a net loss of differentiated cells.

In conclusion, our work has uncovered loss-of-function biallelic germline *CDK10* mutations as responsible for a growth-retardation syndrome. This congenital disease of stunted growth can be modeled in *Cdk10*-deficient mice. Our work suggests that deregulation of metabolic pathways could in part explain the growth restriction seen in the absence of CDK10. These unanticipated effects of CDK10 on metabolism could lead to context- or lineage-dependent arrest of cell growth and could involve transduction of signals at the level of the cilia. Future work should strive to better explain the pathogenesis of Al Kaissi syndrome with the aim of creating possible therapeutic interventions.

Accession Numbers

Microarray data were deposited in the Gene Expression Omnibus under accession number GEO: GSE98628.

Supplemental Data

Supplemental Data include seven figures and five tables and can be found with this article online at http://dx.doi.org/10.1016/j.ajhg.2017.08.003.

Acknowledgments

We thank all families for partaking in this study. This work is the result of a fruitful collaboration between several research groups, and therefore it is difficult to give sufficient credit to each author. Nevertheless, the Kaldis, Reversade, and Al Kaissi laboratories contributed equally. The authors would also like to thank Isabelle Dalle Fusine and all past and current members of the Kaldis, Reversade, Windpassinger, and Al Kaissi labs for technical assistance and fruitful discussions. We acknowledge the technical expertise provided by the Advanced Molecular Pathology Laboratory at the Institute of Molecular and Cell Biology. We are grateful to Eileen Southon and Susan Reid for help in generating the *Cdk10*^{flox} mice. This work was supported by the Intramural Research Program of the NIH, the National Cancer Institute, and the Center for Cancer Research (V.C. and L.T.); a Strategic Positioning Fund

for the Genetic Orphan Diseases program (SPF2012/005) and an Industry Alignment Fund for the Singapore Childhood Undiagnosed Diseases program (IAF311019) from the A*STAR (Agency for Science, Technology, and Research) Biomedical Research Council (B.R.); and the A*STAR Biomedical Research Council (P.K.).

Received: May 10, 2017
Accepted: August 1, 2017
Published: September 7, 2017

Web Resources

1000 Genomes, http://www.1000genomes.org/
ANNOVAR, http://annovar.openbioinformatics.org/en/latest/
BLAST, http://blast.ncbi.nlm.nih.gov/Blast.cgi
ClinVar, ftp://ftp.ncbi.nlm.nih.gov/pub/clinvar/vcf_GRCh37/
Database of Genomic Variants, http://projects.tcag.ca/variation/
dbSNP146, http://www.ncbi.nlm.nih.gov/snp
dCHIP software, http://www.dchip.org/
ExAC Browser, http://exac.broadinstitute.org/
GeneMatcher, https://genematcher.org/
Human Splicing Finder, http://www.umd.be/HSF/
NHLBI Exome Sequencing Project (ESP) Exome Variant Server, http://evs.gs.washington.edu/EVS/
OMIM, http://www.omim.org/
PolyPhen-2, http://genetics.bwh.harvard.edu/pph2/
UCSC Genome Browser, http://genome.ucsc.edu/

References

1. Lim, S., and Kaldis, P. (2013). Cdks, cyclins and CKIs: roles beyond cell cycle regulation. Development *140*, 3079–3093.
2. Malumbres, M., Harlow, E., Hunt, T., Hunter, T., Lahti, J.M., Manning, G., Morgan, D.O., Tsai, L.H., and Wolgemuth, D.J. (2009). Cyclin-dependent kinases: a family portrait. Nat. Cell Biol. *11*, 1275–1276.
3. Morgan, D.O. (2007). The cell cycle: principles of control (New Science Press Ltd).
4. Brambilla, R., and Draetta, G. (1994). Molecular cloning of PISSLRE, a novel putative member of the cdk family of protein serine/threonine kinases. Oncogene *9*, 3037–3041.
5. Graña, X., Claudio, P.P., De Luca, A., Sang, N., and Giordano, A. (1994). PISSLRE, a human novel CDC2-related protein kinase. Oncogene *9*, 2097–2103.
6. Kasten, M., and Giordano, A. (2001). Cdk10, a Cdc2-related kinase, associates with the Ets2 transcription factor and modulates its transactivation activity. Oncogene *20*, 1832–1838.
7. Guen, V.J., Gamble, C., Flajolet, M., Unger, S., Thollet, A., Ferandin, Y., Superti-Furga, A., Cohen, P.A., Meijer, L., and Colas, P. (2013). CDK10/cyclin M is a protein kinase that controls ETS2 degradation and is deficient in STAR syndrome. Proc. Natl. Acad. Sci. USA *110*, 19525–19530.
8. Boczek, N.J., Kruisselbrink, T., Cousin, M.A., Blackburn, P.R., Klee, E.W., Gavrilova, R.H., and Lanpher, B.C. (2017). Multigenerational pedigree with STAR syndrome: A novel FAM58A variant and expansion of the phenotype. Am. J. Med. Genet. A. *173*, 1328–1333.
9. Unger, S., Böhm, D., Kaiser, F.J., Kaulfuss, S., Borozdin, W., Buiting, K., Burfeind, P., Böhm, J., Barrionuevo, F., Craig, A., et al. (2008). Mutations in the cyclin family member FAM58A cause an X-linked dominant disorder characterized by syndactyly, telecanthus and anogenital and renal malformations. Nat. Genet. *40*, 287–289.
10. Guen, V.J., Gamble, C., Perez, D.E., Bourassa, S., Zappel, H., Gärtner, J., Lees, J.A., and Colas, P. (2016). STAR syndrome-associated CDK10/Cyclin M regulates actin network architecture and ciliogenesis. Cell Cycle *15*, 678–688.
11. Yeh, C.W., Kao, S.H., Cheng, Y.C., and Hsu, L.S. (2013). Knockdown of cyclin-dependent kinase 10 (cdk10) gene impairs neural progenitor survival via modulation of raf1a gene expression. J. Biol. Chem. *288*, 27927–27939.
12. Lin, Y.J., Liao, W.L., Wang, C.H., Tsai, L.P., Tang, C.H., Chen, C.H., Wu, J.Y., Liang, W.M., Hsieh, A.R., Cheng, C.F., et al. (2017). Association of human height-related genetic variants with familial short stature in Han Chinese in Taiwan. Sci. Rep. *7*, 6372.
13. Wölfel, T., Hauer, M., Schneider, J., Serrano, M., Wölfel, C., Klehmann-Hieb, E., De Plaen, E., Hankeln, T., Meyer zum Büschenfelde, K.H., and Beach, D. (1995). A $p16^{INK4a}$-insensitive CDK4 mutant targeted by cytolytic T lymphocytes in a human melanoma. Science *269*, 1281–1284.
14. Zuo, L., Weger, J., Yang, Q., Goldstein, A.M., Tucker, M.A., Walker, G.J., Hayward, N., and Dracopoli, N.C. (1996). Germline mutations in the $p16^{INK4a}$ binding domain of CDK4 in familial melanoma. Nat. Genet. *12*, 97–99.
15. Hussain, M.S., Baig, S.M., Neumann, S., Peche, V.S., Szczepanski, S., Nürnberg, G., Tariq, M., Jameel, M., Khan, T.N., Fatima, A., et al. (2013). CDK6 associates with the centrosome during mitosis and is mutated in a large Pakistani family with primary microcephaly. Hum. Mol. Genet. *22*, 5199–5214.
16. Fujita, P.A., Rhead, B., Zweig, A.S., Hinrichs, A.S., Karolchik, D., Cline, M.S., Goldman, M., Barber, G.P., Clawson, H., Coelho, A., et al. (2011). The UCSC Genome Browser database: update 2011. Nucleic Acids Res. *39*, D876–D882.
17. Kent, W.J., Sugnet, C.W., Furey, T.S., Roskin, K.M., Pringle, T.H., Zahler, A.M., and Haussler, D. (2002). The human genome browser at UCSC. Genome Res. *12*, 996–1006.
18. Lin, M., Wei, L.J., Sellers, W.R., Lieberfarb, M., Wong, W.H., and Li, C. (2004). dChipSNP: significance curve and clustering of SNP-array-based loss-of-heterozygosity data. Bioinformatics *20*, 1233–1240.
19. Diril, M.K., Ratnacaram, C.K., Padmakumar, V.C., Du, T., Wasser, M., Coppola, V., Tessarollo, L., and Kaldis, P. (2012). Cyclin-dependent kinase 1 (Cdk1) is essential for cell division and suppression of DNA re-replication but not for liver regeneration. Proc. Natl. Acad. Sci. USA *109*, 3826–3831.
20. Lee, E.-C., Yu, D., Martinez de Velasco, J., Tessarollo, L., Swing, D.A., Court, D.L., Jenkins, N.A., and Copeland, N.G. (2001). A highly efficient *Escherichia coli*-based chromosome engineering system adapted for recombinogenic targeting and subcloning of BAC DNA. Genomics *73*, 56–65.
21. Rodríguez, C.I., Buchholz, F., Galloway, J., Sequerra, R., Kasper, J., Ayala, R., Stewart, A.F., and Dymecki, S.M. (2000). High-efficiency deleter mice show that FLPe is an alternative to CreloxP. Nat. Genet. *25*, 139–140.
22. Lewandoski, M., Meyers, E.N., and Martin, G.R. (1997). Analysis of Fgf8 gene function in vertebrate development. Cold Spring Harb. Symp. Quant. Biol. *62*, 159–168.
23. Truett, G.E., Heeger, P., Mynatt, R.L., Truett, A.A., Walker, J.A., and Warman, M.L. (2000). Preparation of PCR-quality mouse genomic DNA with hot sodium hydroxide and tris (HotSHOT). Biotechniques *29*, 52–54, 54.

24. Koh, H.W., Swa, H.L., Fermin, D., Ler, S.G., Gunaratne, J., and Choi, H. (2015). EBprot: Statistical analysis of labeling-based quantitative proteomics data. Proteomics *15*, 2580–2591.
25. Herwig, R., Hardt, C., Lienhard, M., and Kamburov, A. (2016). Analyzing and interpreting genome data at the network level with ConsensusPathDB. Nat. Protoc. *11*, 1889–1907.
26. Todaro, G.J., and Green, H. (1963). Quantitative studies of the growth of mouse embryo cells in culture and their development into established lines. J. Cell Biol. *17*, 299–313.
27. Berthet, C., Aleem, E., Coppola, V., Tessarollo, L., and Kaldis, P. (2003). Cdk2 knockout mice are viable. Curr. Biol. *13*, 1775–1785.
28. Sobreira, N., Schiettecatte, F., Valle, D., and Hamosh, A. (2015). GeneMatcher: a matching tool for connecting investigators with an interest in the same gene. Hum. Mutat. *36*, 928–930.
29. Crawford, J., Ianzano, L., Savino, M., Whitmore, S., Cleton-Jansen, A.M., Settasatian, C., d'apolito, M., Seshadri, R., Pronk, J.C., Auerbach, A.D., et al. (1999). The PISSLRE gene: structure, exon skipping, and exclusion as tumor suppressor in breast cancer. Genomics *56*, 90–97.
30. Sergère, J.C., Thuret, J.Y., Le Roux, G., Carosella, E.D., and Leteurtre, F. (2000). Human CDK10 gene isoforms. Biochem. Biophys. Res. Commun. *276*, 271–277.
31. Diril, M.K., Bisteau, X., Kitagawa, M., Caldez, M.J., Wee, S., Gunaratne, J., Lee, S.H., and Kaldis, P. (2016). Loss of the Greatwall kinase weakens the spindle assembly checkpoint. PLoS Genet. *12*, e1006310.
32. Puchalska, P., and Crawford, P.A. (2017). Multi-dimensional roles of ketone bodies in fuel metabolism, signaling, and therapeutics. Cell Metab. *25*, 262–284.
33. Guen, V.J., Gamble, C., Lees, J.A., and Colas, P. (2017). The awakening of the CDK10/Cyclin M protein kinase. Oncotarget *8*, 50174–50186.
34. Stowe, T.R., Wilkinson, C.J., Iqbal, A., and Stearns, T. (2012). The centriolar satellite proteins Cep72 and Cep290 interact and are required for recruitment of BBS proteins to the cilium. Mol. Biol. Cell *23*, 3322–3335.
35. Hernandez-Hernandez, V., Pravincumar, P., Diaz-Font, A., May-Simera, H., Jenkins, D., Knight, M., and Beales, P.L. (2013). Bardet-Biedl syndrome proteins control the cilia length through regulation of actin polymerization. Hum. Mol. Genet. *22*, 3858–3868.
36. Sumarsono, S.H., Wilson, T.J., Tymms, M.J., Venter, D.J., Corrick, C.M., Kola, R., Lahoud, M.H., Papas, T.S., Seth, A., and Kola, I. (1996). Down's syndrome-like skeletal abnormalities in Ets2 transgenic mice. Nature *379*, 534–537.

The American Journal of Human Genetics, Volume *101*

Supplemental Data

CDK10 Mutations in Humans and Mice Cause Severe Growth Retardation, Spine Malformations, and Developmental Delays

Christian Windpassinger, Juliette Piard, Carine Bonnard, Majid Alfadhel, Shuhui Lim, Xavier Bisteau, Stéphane Blouin, Nur'Ain B. Ali, Alvin Yu Jin Ng, Hao Lu, Sumanty Tohari, S. Zakiah A. Talib, Noémi van Hul, Matias J. Caldez, Lionel Van Maldergem, Gökhan Yigit, Hülya Kayserili, Sameh A. Youssef, Vincenzo Coppola, Alain de Bruin, Lino Tessarollo, Hyungwon Choi, Verena Rupp, Katharina Roetzer, Paul Roschger, Klaus Klaushofer, Janine Altmüller, Sudipto Roy, Byrappa Venkatesh, Rudolf Ganger, Franz Grill, Farid Ben Chehida, Bernd Wollnik, Umut Altunoglu, Ali Al Kaissi, Bruno Reversade, and Philipp Kaldis

Supplemental Note: Case Reports

We report here the clinical, genetic and molecular aetiology of a previously unidentified syndrome in individuals with mutations in *CDK10* (MIM:603464).

In Family 1, two affected male siblings were born to Tunisian consanguineous healthy parents. The proband (F1-II:1) was a six year old male child who was referred because of torticollis. He was born to a 28 years old woman and 32 years old first cousin man after full term gestation. At birth, he was hypotonic, displayed intrauterine growth retardation and his subsequent course of development has been of severe retardation in all aspects of development. Extreme hypotonia and profound muscular weakness suggested the diagnosis of a neuromuscular disease, which was not confirmed by tests. Clinical examination of the proband revealed short stature (-4SD), large head (50th percentile) in comparison to his small body. In addition to persistent torticollis, he presented with craniofacial anomalies including synophrys, hypertelorism, ptosis, narrow forehead, depressed nasal bridge, large bulky nose, long philtrum, along with a thin upper lip (Figure 1B, Table 1, and Table S1). To understand the aetiology behind the persistent torticollis, we performed 3D reconstruction CT scans which indicated incomplete development of the posterior arches of the atlas (clefting-arrow) and fusion of the left posterior arch of the atlas with the body of the axis indicative of a massive upper cervical malsegmentation (Figure 1D).

Under the assumption of an autosomal recessive inheritance both affected brothers were investigated for shared homozygosity-by-descent (HBD) regions. Using Affymetrix GeneChip Human Mapping 250K NspI array data and the dCHIP software, we were able to identify a ~5 Mbp HBD region on the very distal part of chromosome 16 (data not shown). Subsequent whole exome sequencing revealed the presence of a homozygous splice site mutation c.609-1G>A (NM_052988.4) disrupting the splice acceptor site of intron 8 of *CDK10* in the affected family members (Figure 1A, 1G, and S1), which is present in a heterozygous state in the tested mother. This mutation (rs767176610, dbSNP) has an allele frequency of 2.488e-05 and has not been found before in a homozygous state (ExAC database).

In Family 2, two affected male siblings were born to Algerian first cousins (Figure 1A). The oldest one (F2-II:4) had intrauterine growth retardation. A neonatal respiratory distress and two episodes of seizures at day 4 were observed. His developmental milestones were severely delayed; he walked independently at 30 months and had language delay. His learning disorders required special education. Examination at 7 years indicated growth retardation (-2.5 SD),

normal occipitofrontal head circumference (OFC), a wide-based gait, a sacral dimple, deep palmar creases, and facial dysmorphism including a triangular face, telecanthus, downslanting palpebral fissures, bilateral epicanthal folds, low-set and posteriorly rotated ears, a small chin, and a nevus flammeus of the glabellar region. Brain MRI and cardiac ultrasound were normal (Table 1, Table S1). By 3D reconstruction CT scan, multilayered spinal segmentation defects were observed: C1 anterior clefting, C2-C3 posterior vertebral bodies fusion with laminae and spinous processes fusion, alongside with sacral S2-S5 posterior clefting. In addition a Th4 hemivertebrae fused with posterior processes of Th3 and Th5 was shown. (Figure 1E, from left to right). His younger brother (F2-II:5) was born after an uneventful pregnancy with normal parameters. Atrial septal defect and pulmonary artery stenosis were diagnosed in the neonatal period. He walked independently at 4 years and had no language. He was also a slow learner requiring special education. Examination at 5 years was similar to that of his brother in many respects; growth retardation (-3 SD), small OFC (-2 SD), wide-based gait, sacral dimple, deep palmar creases, and the same facial appearance. Kidney ultrasounds were normal in both individuals and they had no hearing or visual impairment. Array-CGH analysis with a resolution of 25 kb, revealed a small (2.6-28 kb) homozygous microdeletion of 16q24.3 encompassing exons 2 and 3 of *CDK10*, designated ISCN 2009: arr 16q24.3 89,754,790 -89,757,400 x 0 (hg19) in the two affected individuals (Figure 1G). Quantitative PCR (qPCR) analysis confirmed the 16q24.3 microdeletion (data not shown). Segregation analysis indicated the presence of the deletion in the heterozygous state in the parents and three healthy siblings of the index cases (Figure 1A).

Family 3 is a Saudi family with one affected child (F3-II:2) and one healthy sibling born to consanguineous parents. The proband was referred for evaluation due to severe hydrocephalus with dilated ventricles, thinning of the corpus callosum, and absence of the septum pellucidum, which was diagnosed antenatally by ultrasound. At birth she was hypotonic with marked hydrocephalus, dysmorphic features, and a sacral dimple. Birth weight was 2.9 kg (-1 SD). Brain and whole spine MRI confirmed the diagnosis of supratentorial hydrocephalus with partial agenesis of the corpus callosum and normal spine. Further radiological investigations indicated bilateral nephrocalcinosis and a small atrial septal defect. Later, the individual had recurrent attacks of chest infection demanding recurrent pediatric intensive care unit (PICU) admissions. At 18 months of age she was referred to the genetic facility for further investigations with a length 75 cm (-1.3 SD), weight 8.4 kg (-0.2 SD) and head circumference at 50 cm (3 SD). She had dysmorphic features; high arched palate, brachycephaly, synophrys, low set ears, and broad forehead in addition to the marked hydrocephalus. Detailed metabolic workup was requested including plasma amino acids, urine organic acids and very long chain fatty acids but were all

within normal limits. Currently the individual is 40 months old and started to walk independently. She underwent ventriculoperitoneal shunt insertion and developed seizure, which was well controlled with antiepileptic medications. Karyotyping was normal and CGH microarray indicated homozygosity blocks and no pathogenic changes. Whole exome sequencing was requested and revealed a homozygous c.139delG in exon 2 of *CDK10*, resulting in a truncated protein p.Glu47ArgfsTer21. Both parents were heterozygous for the same mutation. This *CDK10* variant is predicted to cause loss of normal protein function either through protein truncation or nonsense-mediated mRNA decay.

Family 4 is a consanguineous family with three affected members from two separate branches (Figure 1A). Two affected siblings from the first branch were referred for evaluation due to similar facial dysmorphisms (Figure 1B), developmental delay, intellectual disability, and congenital hypothyroidism. The index case (F4-II:1) was the first-born child of first cousin parents of Kurdish descent, originating from Southeastern Turkey. Following an uneventful pregnancy, he was born by normal spontaneous cephalic delivery at term, with a birth weight of 2950 gr (-1.1 SD). Hypotonia was noted at birth and he was interned at level I neonatal care on the fourth postnatal day, due to poor sucking, restlessness, and regurgitations. He was diagnosed with congenital hypothyroidism and thyroid replacement therapy was started. Between 12 months and 3 years of age, he was hospitalized nine times due to lower respiratory tract infections and reactive airway. A work-up comprising viral serology, complete blood count, lymphocyte subset analysis, serum immunoglobulin levels, and sweat test showed results within the normal range. The severity of the infections diminished after age three and the family did not report any infections after the age of seven. He had a febrile seizure at the age of 3 years, during a hospital stay due to pneumonia. Electroencephalogram and cranial MRI results were normal at this time. Neurodevelopmental milestones were significantly delayed; he sat without support at 18 months of age, walked independently at 42 months, used first two-word sentences at 4 years of age, and did not have sphincter control until 6 years of age (Table 1, Table S1). At 8 1/2 years of age, his weight was 12.2 kg (-4.7 SD), height 106 cm (-4.4 SD), and OFC 46.5 cm (-4.6 SD). He had a happy demeanor during examination, was cooperative, but had short attention span. Physical evaluation indicated thick, bushy hair, abnormal hair patterning with two hair whorls on the frontal hairline, bilateral epicanthus tarsalis, upslanting palpebral fissures, mild malar rash, wide nasal bridge and ridge, broad nasal tip with short columella, smooth and long philtrum, thin vermilion of upper and lower lips, high and narrow palate, pointed chin, bilaterally low-set, posteriorly rotated ears with angulated helices, prominent antihelix stems, underdeveloped superior crura, and hypoplastic lobules (Figure 1B). He had doughy, mildly hyperextensible skin, hyperextensibility of the elbow joints and small joints of the hand, small hands with total hand

length of 10.5 cm [<3rd centile], bilateral single palmar flexion crease, fifth finger clinodactyly, bilateral pes planus, broad halluces, and dystrophic toenails (Figure 1C). Hands and feet were cold due to peripheral vasomotor disturbance with episodic cutis marmorata and redness. He had a 5x5 cm patch of hypertrichosis localized on the lumbar area and a sacral dimple. Neurologic and systemic examinations were unremarkable except mildly wide based gait. Detailed metabolic screening including urine and plasma amino acids, urine organic acids, total and free carnitine, acylcarnitine, and oligosaccharides yielded no evidence of an inborn error of metabolism. Full skeletal survey showed fusion of the laminae and pedicles of C2 and C3 vertebrae on the posterior aspects, with rudimentary C2-C3 disk space (Figure 1F) but neck rotation was normal in physical re-evaluation. Using left hand radiograph, bone age was determined to be compatible with 6.5 years. Further work-up comprised routine biochemical screening, evaluation of pituitary axis with basal hormone levels, echocardiography, abdominal and renal ultrasound, audiological evaluation, all with normal results. High-resolution array-CGH using NimbleGen 630 K CGH array did not reveal any major chromosomal anomalies.

Sibling F4-II:2, sister to F4-II:1, was born after an uneventful pregnancy via normal spontaneous delivery at 39 weeks of gestation, with a birth weight of 2280 g (-2.2 SD). Hypothyroidism was noted at 4 months of age, necessitating continuous thyroid hormone replacement. Other pituitary deficiencies were ruled out. She was hospitalized eight times due to lower respiratory tract infections between the age 12 months and 5 years. Immunologic workup at 2 years of age, as performed for her affected brother F4-II:1, failed to demonstrate an underlying immune defect. She had a febrile seizure at the age of 4 years but electroencephalogram and cranial MRI findings were normal. Neurodevelopmental milestones were significantly delayed; she sat without support at 20 months of age, walked independently at 35 months, used first two-word sentences at 5 years of age, and did not have sphincter control until the age of 7 (Table 1, Table S1). At 7 years 3 months, her weight was 11.5 kg (-4.2 SD), height 97.5 cm (-4.7 SD), and OFC 46 cm (-4.4 SD). Dysmorphic facial features included thick and woolly hair, midline capillary hemangiomata on the glabella and on the inferior nuchal region, bilateral epicanthus tarsalis and telecanthus, upslanting palpebral fissures, malar rash, wide nasal bridge and ridge, broad nasal tip, smooth and long philtrum, thin upper lip vermilion, high and narrow palate, pointed chin, bilaterally low-set, posteriorly rotated ears with angulated helices, prominent antihelix stems, underdeveloped superior crura, underdeveloped tragi, prominent antitragi, and hypoplastic lobules (Figure 1B). She had easily bruised, doughy skin, hyperextensible small joints of the hand, small hands with total hand length of 10.3 cm [<3rd centile], bilateral fifth finger clinodactyly, diastasis recti with prominent umbilicus, sacral dimple and bilateral broad halluces. Hands and feet were cold with episodic cutis marmorata and

redness. Neurologic and systemic examination was otherwise unremarkable, with no motor weakness or sensory deficit. Denver II developmental test performed at the chronological age of 7 years 3 months suggested gross motor skills compatible with 44 months, fine motor skills with 22 months, personal-social skills with 25 months, and language skills with 36 months. Eye and fundus examination, a routine biochemical screen, detailed metabolic screening, echo-cardiography, abdominal and renal ultrasonography, chromosome analysis at 500-550 band levels revealed normal results. Full skeletal survey indicated the fusion of the posterior elements of the C2 and C3, with underdeveloped vertebral body of atlas, and atlantoaxial instability. Using left hand radiograph, bone age was determined to be compatible with 5 years.

The affected cousin F4-II:3 was not evaluated in the clinics. History, clinical data, and photographs suggested that he was similarly affected as his affected cousins. He was born via normal spontaneous delivery at 38 weeks of gestation, with a birth weight of 3120 g (0.6 SD). At 3 years 9 months, his weight was 10.5 kg (-3.4 SD), height 86 cm (-3.5 SD), and OFC 44 cm (-3.9 SD). His development was markedly delayed, sitting unsupported at 24 months, and walking independently at 40 months of age. By 45 months, he could speak with only a few simple words without word combinations. Photographs revealed dysmorphic facial features similar to his cousins, including capillary hemangioma on the glabella, bilateral telecanthus, upslanting palpebral fissures, mild malar rash, wide nasal bridge and ridge, broad nasal tip, smooth and long philtrum, thin upper lip vermilion, high and narrow palate, pointed chin, and bilaterally low-set, posteriorly rotated ears (Figure 1B), and a sacral dimple. He also was reported to have pes planus, frequent upper airway infections and vasomotor disturbance of hands. Biochemical work-up, cranial MRI and radiographic evaluation of the cervical spine could not be performed.

Under the hypothesis of autosomal recessive inheritance, using whole exome sequencing, a homozygous donor splice-site mutation was identified in the intron 8 of *CDK10* (c.608+1G>A, Figure 1A and 1G). This mutation was not annotated in dbSNP or in the ExAC database and was confirmed by Sanger sequencing and found to be homozygous in the three patients but heterozygous in their parents and unaffected sibling (Figure 1A).

Family 5 is a Turkish family with one affected child and a healthy sibling, and reportedly nonconsanguineous parents originating from the same small village. IUGR was noted by ultrasound at the third trimester, pregnancy was otherwise uncomplicated. He was born by elective caeserean section at 40 weeks of gestation, with a birth weight of 2080 g (-2.4 SD), height and OFC at birth are unknown. He was admitted to the neonatal intensive care unit for 10 days due to respiratory distress, necessitating noninvasive oxygen administration. Echo-cardiography at three months of age, and routine follow up thereafter revealed mild, nonprogressive dilatation of the left ventricle, and mild pulmonary stenosis. At 8 months of age,

a diagnostic workup included routine biochemistry, complete blood count, urinalysis, thyroid hormone levels, sweat test, anti-gliadin and anti-endomysial antibodies, detailed metabolic screening, and abdominal sonography, all with normal results. He underwent orchiopexy due to bilateral undescended testes at the age of 12 months. He was hospitalized due to pneumonia at the age of 24 months, and was diagnosed with gastroesophageal reflux disease during the hospital stay, which ameliorated with medical therapy. Neurodevelopmental milestones were moderately delayed; head control was achieved at two months of age, he sat without support at 11 months, walked at 24 months, used first two-word sentences at 2.5 years, and achieved sphincter control at 4 years. Denver II developmental test performed at the chronological age of 4 years 3 months suggested gross motor skills compatible with 24 months, fine motor skills with 24 months, personal-social skills with 24 months, and language skills with 22 months. Cranial and lumbosacral MRI performed at 3 years of age showed normal structures. At 6 years 6 months of age, he was evaluated in the genetic outpatient clinics. His weight was 14.5 kg (-3.5 SD), height 107 cm (-2.6 SD) and OFC 49.5 cm (-2 SD). Physical evaluation showed dolicocephaly, high forehead, flared eyebrows, hypertelorism, telecanthus, bilateral ptosis, esotropia, convex nasal ridge with mildly broad nasal tip, underdeveloped premaxilla, smooth philtrum, thin vermilion of the upper and lower lips, high palate, tall chin, and bilaterally prominent, low-set, posteriorly-rotated ears with absent superior crura. He had hyperextensibility of the small joints, small hands with bilateral 5^{th} finger clinodactyly, palmoplantar hyperkeratosis, shawl scrotum, and a sacral dimple. He was extremely friendly and gregarious during the examination. Systemic examination was otherwise unremarkable. High-resolution array-CGH using NimbleGen 630 K CGH array showed no pathogenic variations. Next a trio whole-exome sequencing was performed and filtering of variants were carried out using the exome analysis pipeline 'Varbank' of the Cologne Center for Genomics (CCG). The same homozygous *CDK10* exon 8 splice site c.608+1G>A mutation found in family 4 was also present in proband of family 5 suggesting a possible a founder mutation. Both parents were heterozygous carriers of this mutation (Figure 1A).

We suggest to name this previously unrecognized congenital disease as Al Kaissi syndrome.

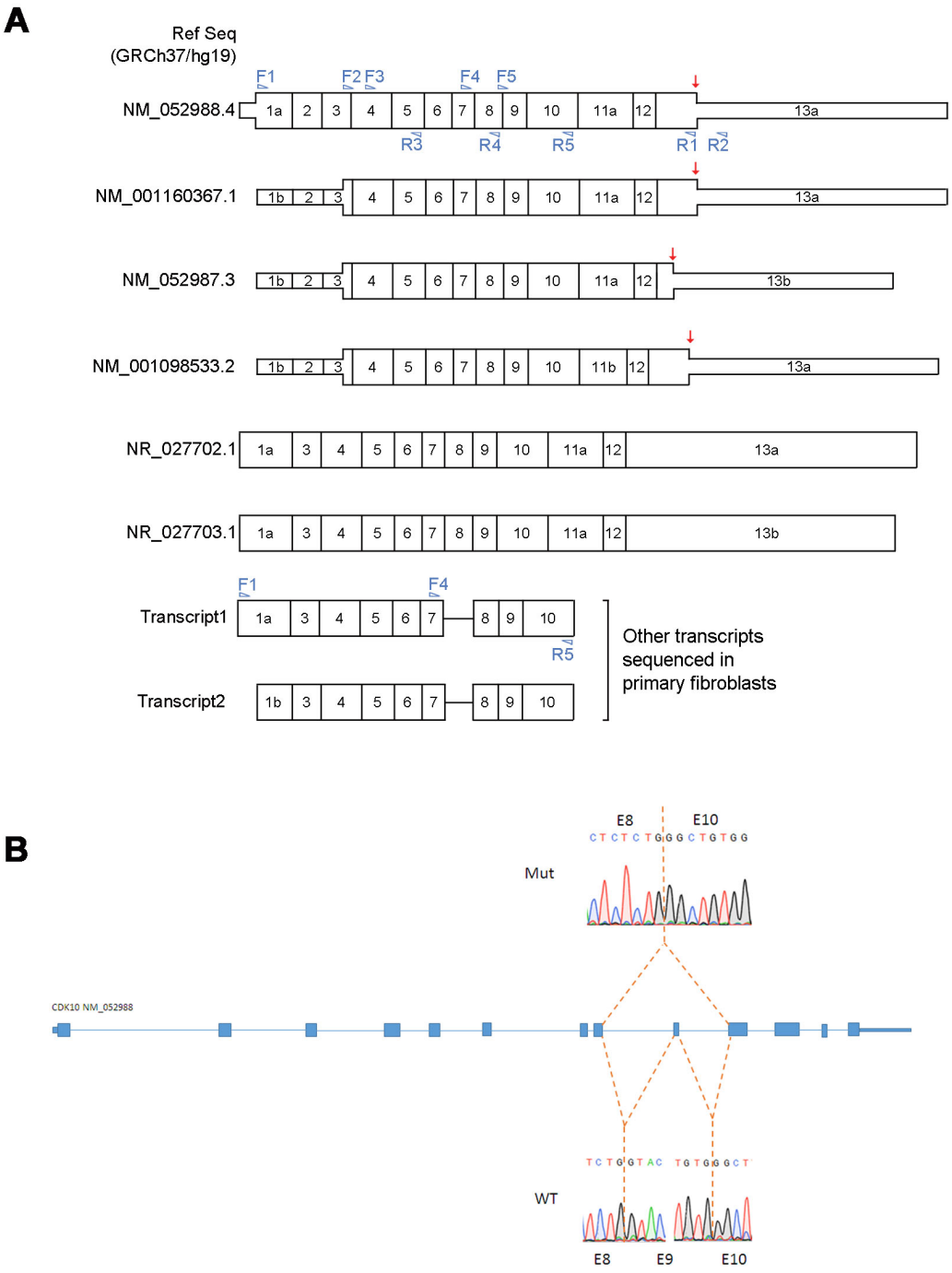

Figure S1: Representation of human Cdk10 transcripts.
(A) Six transcripts for Cdk10 have been described among which 4 are coding (NM_052988, NM_001160367, NM_052987, NM_001098533) and 2 non-coding (NR_027702, NR_027703). Only NM_052988 transcript displays a different start codon for its translation due to a different exon 1; this leads to a longer protein of 360 amino acids due to the translation of a part of the exon 1a, exon 2 and part of the exon 3. Exon 2 and early part of the exon 3 contain the active site of Cdk10 while the cyclin binding motif (PISSLRE) is kept in all transcripts. **(B)** Sequencing of wildtype (WT) and mutant (Mut) transcripts around the exon 8, 9 and 10.

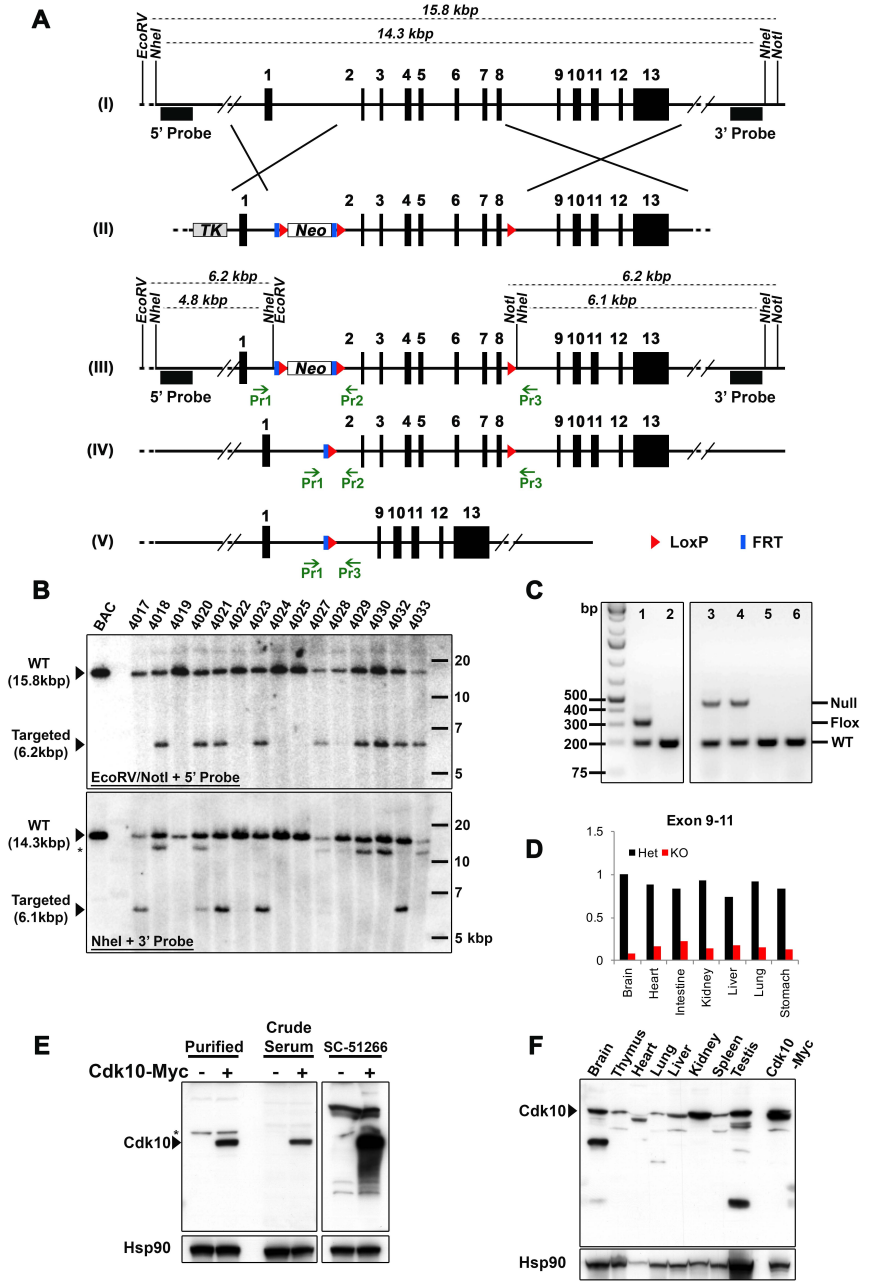

Figure S2: Generation of Cdk10^{flox} mice

(A) To generate Cdk10 knockout, the Cdk10 genomic locus (I, Cdk10^{WT}) was modified in ES cells with the targeting vector (II). A FRT-LoxP-flanked neomycin selection cassette was introduced upstream of exon 2 and a single LoxP recombination site was introduced after exon 8, generating a mutant "Neo" locus (III). Upon expression of FLP recombinase, the neomycin cassette was removed (IV, Cdk10^{Flox}). After Cre recombinase expression, exons 2 to 8 are excised (V, Cdk10^{KO}) resulting in deletion of Cdk10. **(B)** Southern Blotting of selected ES clones after transfection and recombination of the targeting vector. **(C)** Genotyping PCR of obtained different mice harbouring Cdk10^{WT} (WT), Cdk10^{Flox} (Flox) or Cdk10^{KO} (Null) alleles. **(D)** Quantitative RT-PCR of Cdk10 mRNA transcript in different tissues from heterozygous Cdk10$^{WT/KO}$ (Het) and homozygous Cdk10$^{KO/KO}$ (KO) mice. **(E-F)** Immunoblotting of Cdk10 using in house-produced or commercial antibodies on whole cell lysate from non-transfected or transfected NIH3T3 cells **(E)** and from several tissues of Cdk10^{WT} mice **(F)**. HSP90 served as loading control.

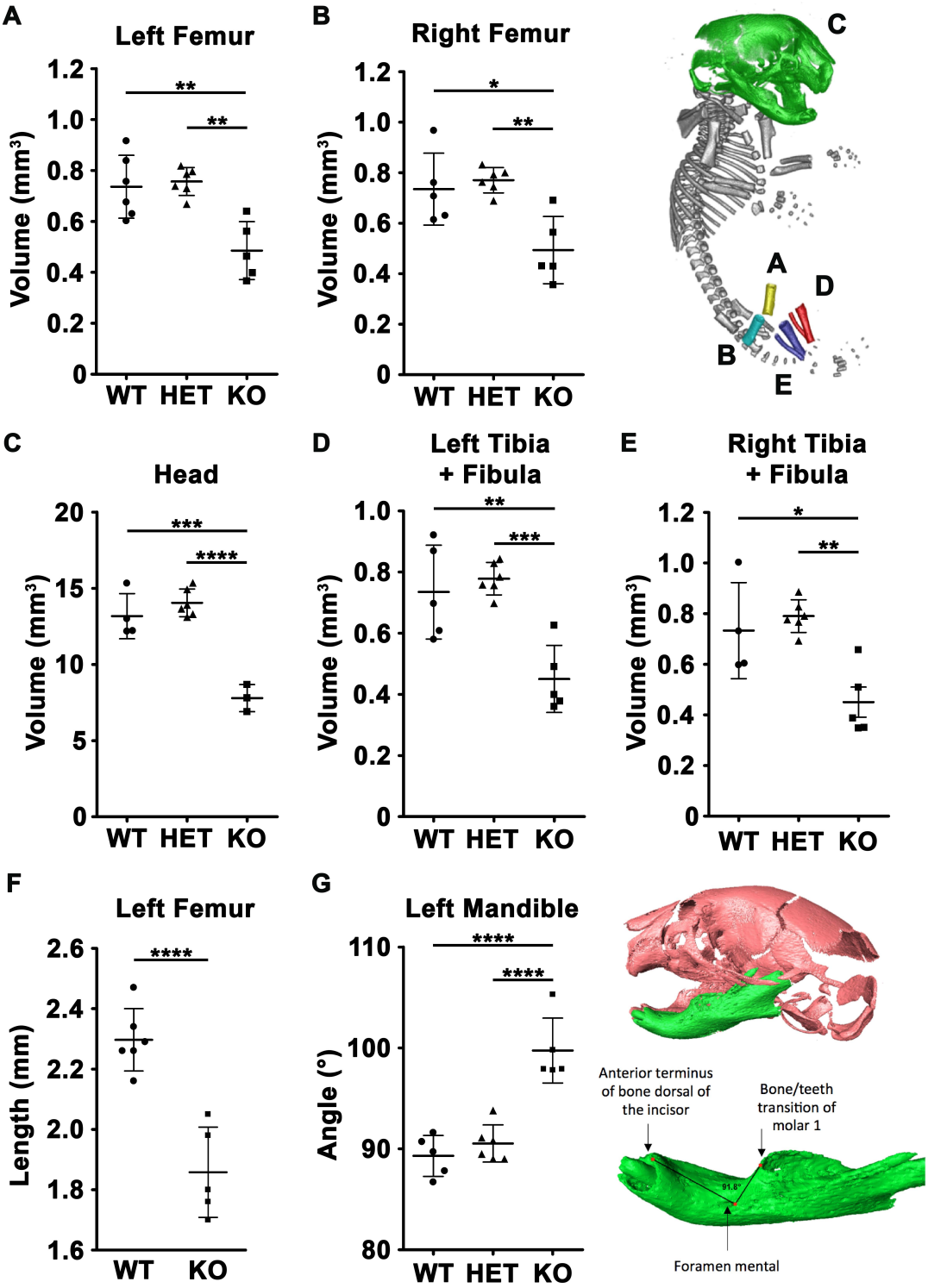

Figure S3: CT scan of mouse skeleton

Measurement of mineralized part from Cdk10$^{WT/WT}$ (WT), heterozygotes Cdk10$^{WT/KO}$ (HET), and knockout Cdk10$^{KO/KO}$ (KO) mice at day P0. Measure of the volume from left **(A)** and right **(B)** femur, the head **(C),** left **(D)** and right **(E)** tibia and fibula. **(F)** Measure of the length of left femur. **(G)** Angle measurement between the anterior terminus of bone dorsal of the incisor, the foramen mental and the bone/teeth transition of molar 1. ANOVA with Tukey's multiple comparison test: * $p<0.05$, ** $p<0.01$, *** $p<0.001$, **** $p<0.0001$. Error bars represent SD.

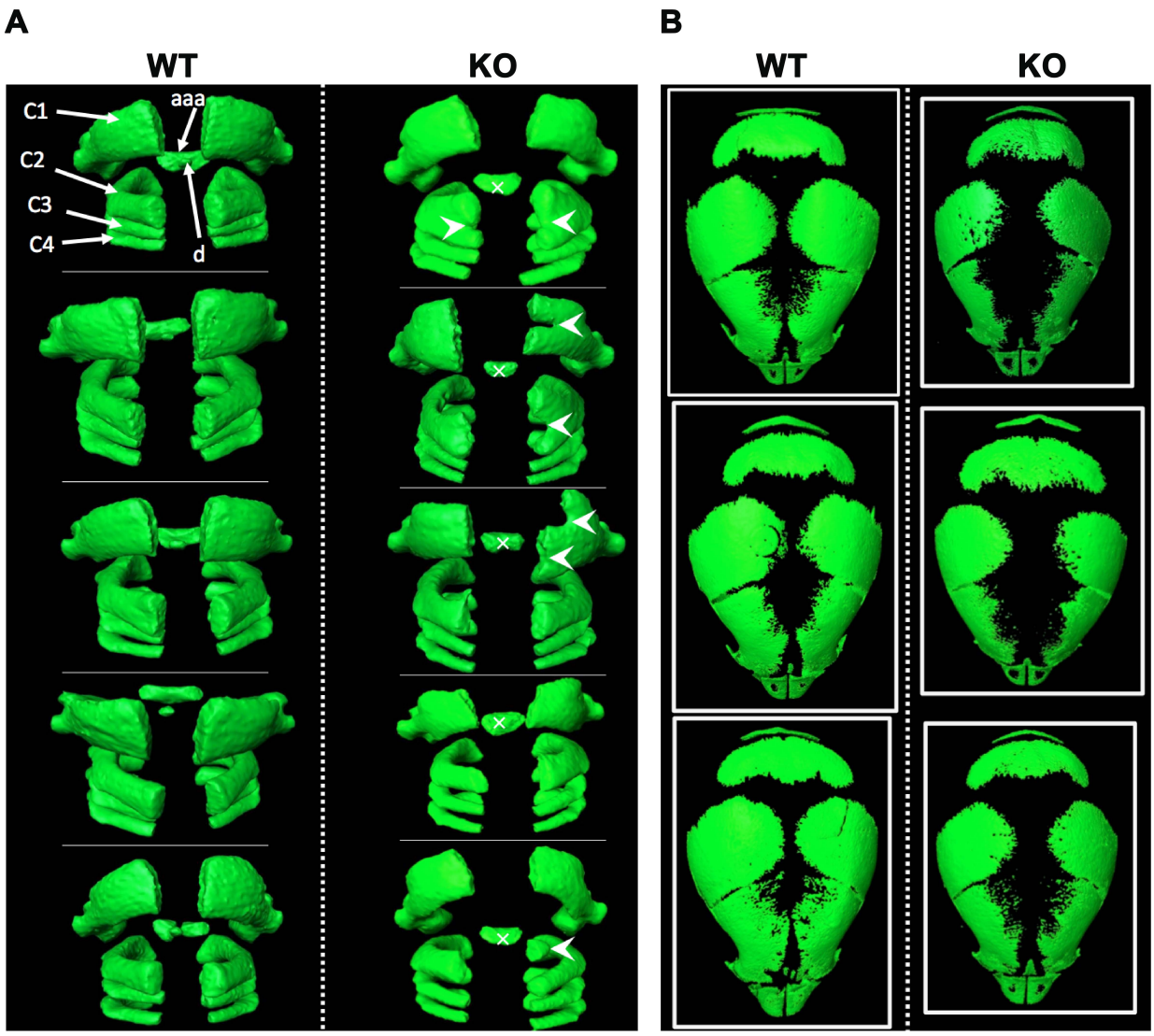

Figure S4: CT scan of vertebrae and skull
(A) Example of posterior 3D visualization of C1 to C4 vertebrae from 5 wild type $Cdk10^{WT/WT}$ (WT) and 5 knockout $Cdk10^{KO/KO}$ (KO) mice. Remarkably, no dens (d) is observed in front of the anterior arch of the atlas (aaa) in the KO animals. The arrows indicate the commonly found bifidity and malsegmentation of the upper cervical vertebral bodies observed in the KO animals. **(B)** Example of skullcap 3D visualization from 3 wild type $Cdk10^{WT/WT}$ (WT) and 3 knockout $Cdk10^{KO/KO}$ (KO) mice. The mineralization of the skullcap appears less accomplished in the KO animals compared to the WT.

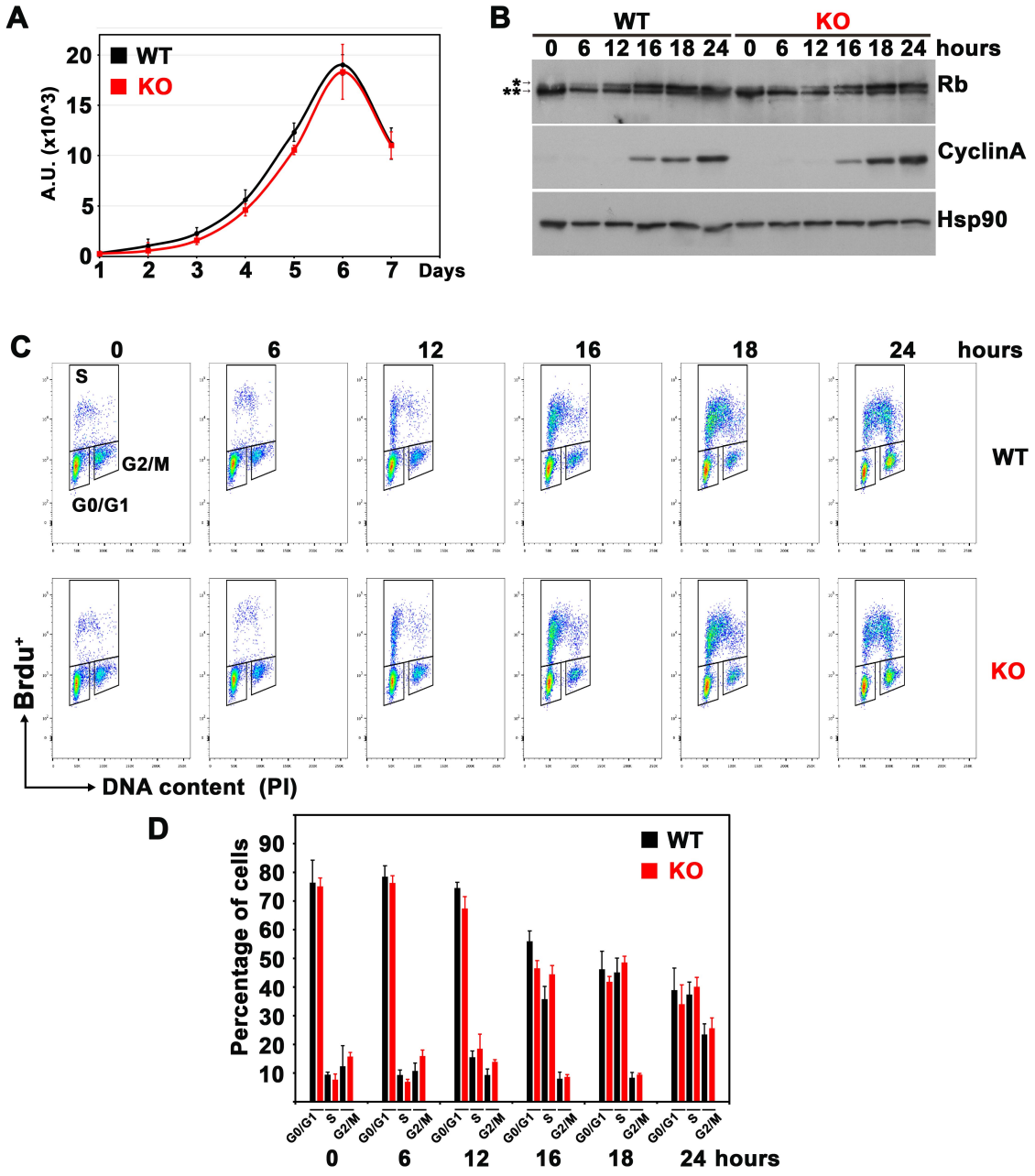

Figure S5: Characterization of Cdk10KO MEFs

(A) Proliferation assay of 3 wild type Cdk10$^{WT/WT}$ (WT) and 3 knockout Cdk10$^{KO/KO}$ (KO) primary MEFs clones. **(B)** Immunoblotting with antibodies against indicated proteins on whole cell lysate from wild type Cdk10$^{WT/WT}$ (WT) and knockout Cdk10$^{KO/KO}$ (KO) primary MEFs collected at different time points after release from serum starvation (G0/G1 synchronization). * and ** indicate hypo- and hyperphosphorylated band of the tumor suppressor Rb, respectively. **(C)** Cdk10$^{WT/WT}$ (WT) and Cdk10$^{KO/KO}$ (KO) MEFs as in (B) were 1hour pulse-labelled with BrdU before collection and analysed by FACS to determine percentage of cells in G0/G1, S, and G2/M phases in a single cell population distributed as BrdU incorporation (BrdU^{+}) versus DNA content (PI). **(D)** Quantitative analysis of 3 wild type Cdk10$^{WT/WT}$ (WT) and 3 knockout Cdk10$^{KO/KO}$ (KO) primary MEFs clones in G0/G1, S, and G2/M phases as represented in (C). Error bars represent SD.

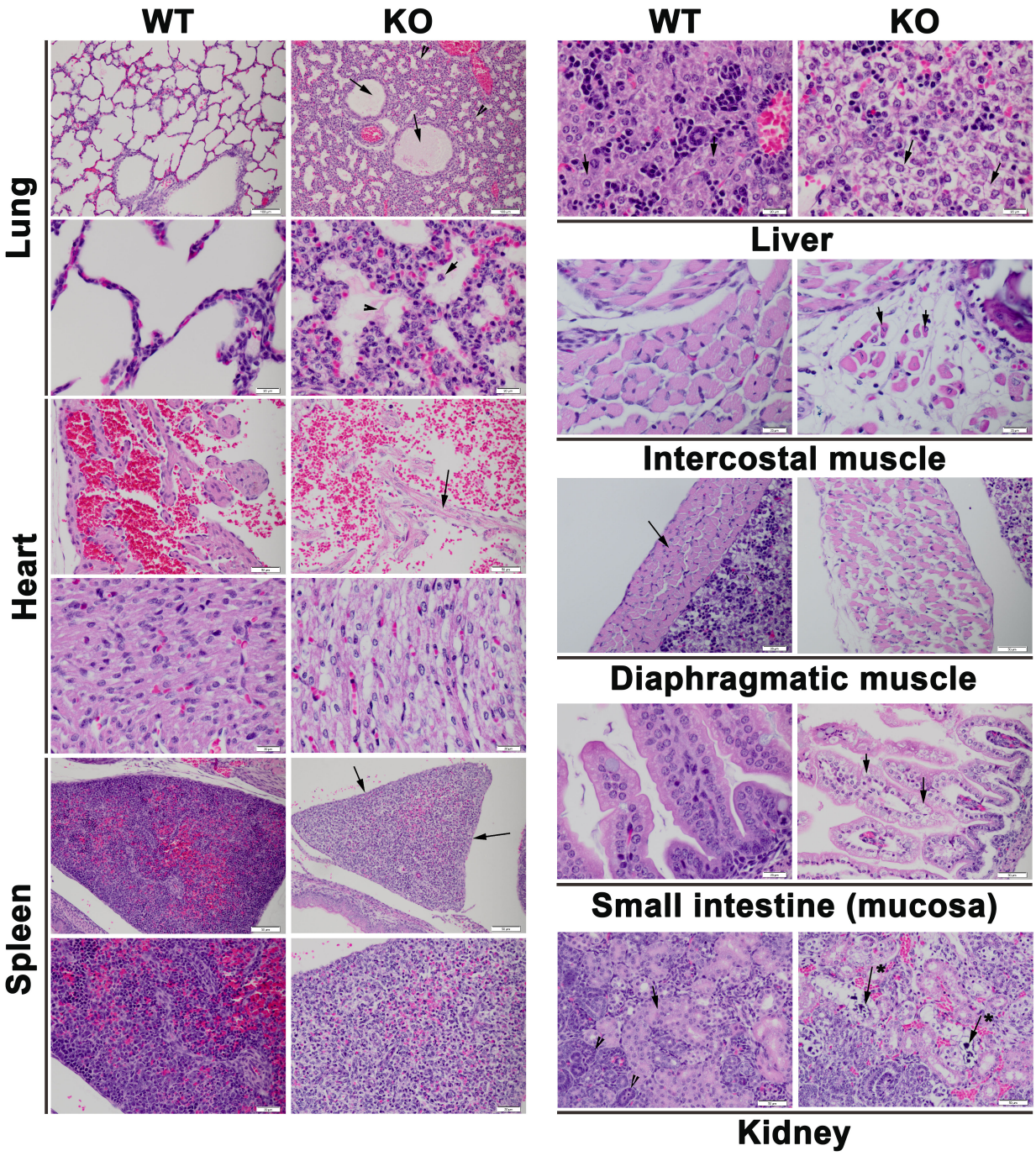

Figure S6: Histology of Cdk10KO mice

H&E stained histological sections of different tissues isolated from wild type $Cdk10^{WT/WT}$ (WT) and knockout $Cdk10^{KO/KO}$ (KO) mice at postnatal day P0.

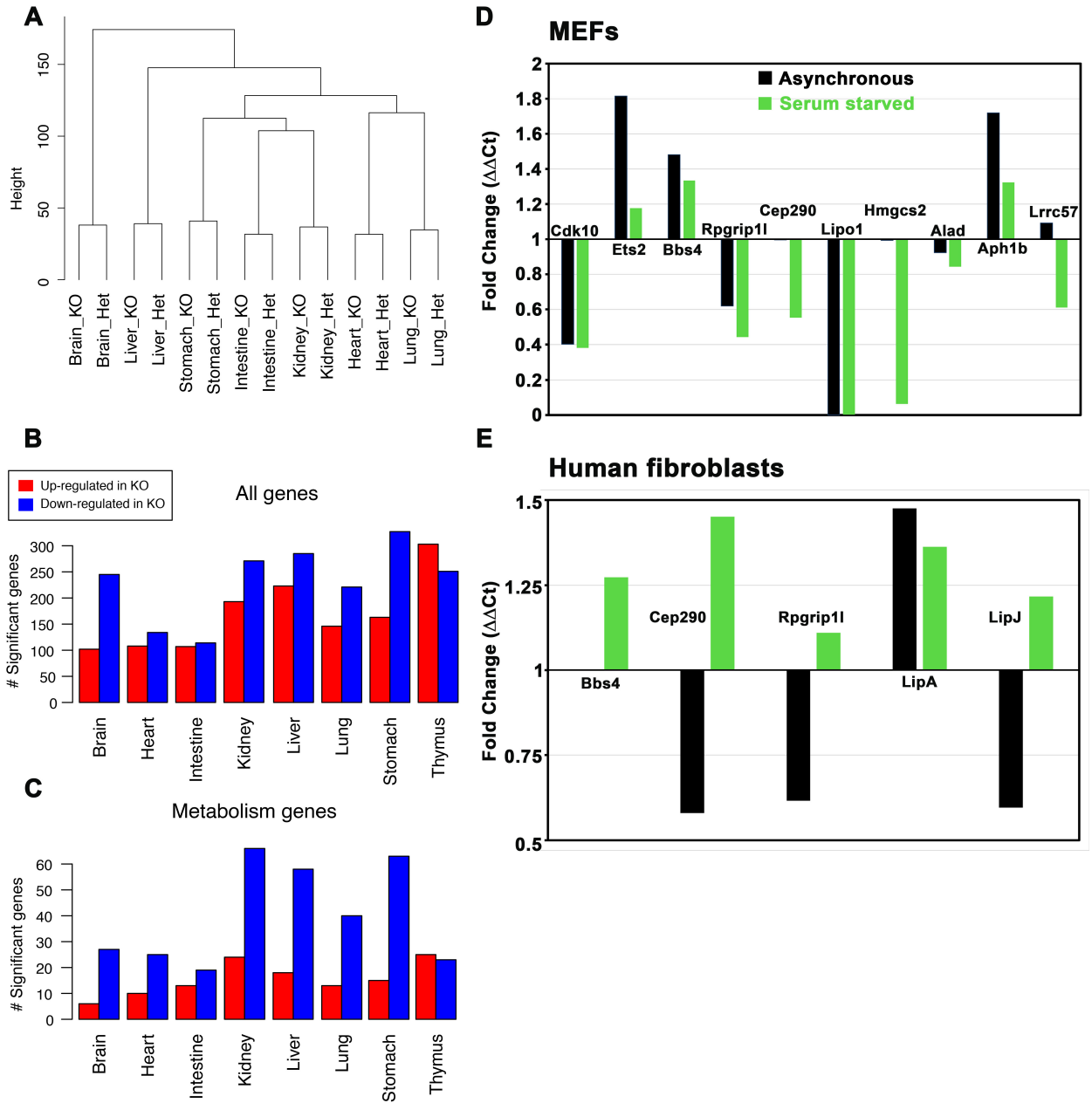

Figure S7: Gene expression analysis of Cdk10KO tissues

(A) Dendrogram of the complete dataset obtained from microarrays of 8 tissues isolated from wild type $Cdk10^{WT/KO}$ (Het) and knockout $Cdk10^{KO/KO}$ (KO) mice at postnatal day P0. **(B-C)** Analysis of the number of genes identified as significantly up- and down-regulated in each tissue in absence of Cdk10. **(D-E)** Quantitative RT-PCR of different transcripts in asynchronous or 96 hours serum starved immortalized MEFs **(D)** or patient-derived fibroblasts **(E).** The bars represent the fold change observed in $Cdk10^{KO/KO}$ (KO) or F4-II:1 individual fibroblasts from the average of 2 primer pairs in comparison to wild type $Cdk10^{WT/WT}$ (WT) or control human fibroblasts after normalization with eEF2 or Gapdh as housekeeping genes using the ΔΔCt method.

Table S5 : Comparison of STAR, BBS and CDK10 syndromes.

	STAR syndrome	*CDK10* syndrome	Bardet-Biedl syndrome
Inheritance pattern	X-linked dominant	autosomal recessive	autosomal recessive
Toe syndactyly	++	-	+
Telecanthus	++	+	-
Anogenital malformations	++	-	++
Renal / urinary tract malformations	++	-	++
Growth retardation	+	++	+
Congenital heart disease	+	+	+
Clinodactyly of 5th finger	+	+	-
Post-axial polydactyly	-	-	++
Dysplastic ears	+	+	-
Hearing loss	+	-	+
Intellectual disability	-	++	++
Cervical spine malformation	-	++	-
Sacral dimple	+	+	-
Obesity	-	-	++
Male hypogonadism	-	-	++
Ocular anomaly	+	-	++ (rod-cone dystrophy)